# SYNTHESIS AND CHARACTERIZATION OF $ZnSe/Co_2SiO_4$ COMPOSITE FOR DEGRADATION OF METHYLENE BLUE (MB) DYES IN WATER

**KAMIL ESLAMAN ABEBAW**

**A THESIS SUBMITED TO THE DEPARTMENT OF MATERIALS SCIENCE AND ENGINEERING SCHOOL OF MECHANICAL, CHEMICAL AND MATERIAL ENGINEERING**

**Presented in Partial Fulfillment of the Requirement for the Degree of Master's in Material science and engineering**

**Office of Graduate Studies**
**Adama Science and Technology University**

**August / 2021**

**Adama, Ethiopia**

# Synthesis and characterization of $ZnSe/Co_2SiO_4$ composite for the degradation of MB dye in water

**Kamil Eslaman Abebaw**

**Advisor: Dinsefa Mensur Andoshe (Ph.D.)**

**A Thesis Submitted to**

**The department of Materials Science and Enigineering**

**School of Mechanical, Chemical, and Materials Engineering**

**Presented in Partial Fulfillment of the Requirement for the Degree of Master's in Materials Science and Engineering**

**Office of Graduate Studies**
**Adama Science and Technology University**

**August / 2021**

## Declaration

I hereby declare that this Master Thesis entitled "Synthesis and characterization of $ZnSe/Co_2SiO_4$ composite for the degradation of Methylene blue (MB) Dye in water" is my original work. That is, it has not been submitted for the award of any academic degree, diploma, or certificate in any other university. All sources of materials that are used for this thesis have been duly acknowledged through citation.

| _____ | _____ | _____ |
|---|---|---|
| Student name | Signature | Date |

## Recommendation

I/we, the advisor(s) of this thesis, hereby certify that I/we have read the revised version of The thesis entitled "**Synthesis and characterization of $ZnSe/Co_2SiO_4$ composite for the degradation of Methylene blue (MB) Dye in water**" prepared under my/our guidance by Kamil Eslaman Abebaw ID: PGR/20811/12, submitted in partial fulfillment of the requirements for the degree of Mater's of Science in Materials Science and Engineering.

Therefore, I/we recommend the submission of revised version of the thesis to the Department following the applicable procedures.

| _____ | _____ | _____ |
|---|---|---|
| Major Advisor | Signature | Date |
| _____ | _____ | _____ |
| Co-advisor | Signature | Date |

# Approval Page

I/we, the advisors of the thesis entitled "Synthesis and characterization of $ZnSe/Co_2SiO_4$ composite for the degradation of Methylene blue (MB) Dye in water" and developed by Kamil Eslaman Abebaw ID: PGR/20811/12, hereby certify that the recommendation and suggestions made by the board of examiners are appropriately incorporated into the final version of the thesis.

| | | |
|---|---|---|
| Major Advisor | Signature | Date |
| Co-advisor | Signature | Date |

We, the undersigned, members of the Board of Examiners of the thesis by Kamil Eslaman Abebaw ID No:PGR/20811/12, have read and evaluated the thesis entitled "**Synthesis and characterization of $ZnSe/Co_2SiO_4$ composite for the degradation of Methylene blue (MB) Dye in water**" and examined the candidate during open defense. This is, therefore, to certify that the thesis is accepted for partial fulfillment of the requirement of the degree of Master of Science in Materials Science and Engineering.

| | | |
|---|---|---|
| Chairperson | Signature | Date |
| Internal Examiner | Signature | Date |
| External Examiner | Signature | Date |

Finally, approval and acceptance of the thesis is contingent upon submission of its final Copy to the Office of Postgraduate Studies (OPGS) through the Department Graduate Council (DGC) and School Graduate Committee (SGC).

| | | |
|---|---|---|
| Department Head | Signature | Date |
| School Dean | Signature | Date |
| Office of Postgraduate Studies, Dean | Signature | Date |

## Acknowledgement

First and foremost, all praises to be the Almighty god ALLAH, whose many blessings have made me who I am today. I would like to thank Adama Science and Technology University ASTU/SM-R/210/21 for financial support. I would also like to express my special thanks of gratitude to my advisor Dr. Dinsefa Mensur who guided me throughout this research. I would like to thank my co-advisor Dr.bely brhane for his guidance and important comments. I am grateful to all of those with whom I have had the pleasure to work during this research. Each of my classmates has provided me extensive personal and professional guidance and taught me a great deal about both scientific research and life in general. I would especially like to thank Mr. Demeke tesfaye for his help during sample characterization. I am very much thankful to my wife Hanan Frew for her love, understanding, prayers and continuing support to complete this research work. I would like to thank my parents, whose love and guidance are with me in whatever I pursue, they are the ultimate role models.

## Table of Contents

Declaration……...……..……ii
Recommendation…….....iii
Approval sheet…….……....iv
Aknoladgnment……..……v
Lest of figures……..……...vi-vii
Last of tables…….…viii
Lest of acronym and symbols…….……..ix
Abstract……..……x
Chapter One.....1
Introduction .....1
1.1 Background.....1
1.2 statement of the problem.....3
1.3 General Objective .....4
1.3.1 Specific Objective .....4
13.2 Significance of the study.....4
Chapter 2 .....5
Literature Review .....5
2.1 Water Pollution.....5
2.2 Methods of Wastewater Treatment.....6
2.3 Mechanism of photocatalysis dye degradation.....7
2.4 Semiconductor Heterojunction photocatalysts .....8
2.4.1 Conventional hetrojunction.....9
2.5 Photocatalytic Semiconductors.....10
2.6 Photocatalitic property of ZnSe .....11

2.7 Photocatalitic property of Co2SiO4 ..... 11
2.8 Parameters affecting photocatalytic activity ..... 12
2.8.1 Calcination temperature ..... 12
2.8.2 Concentration and nature of pollutants ..... 12
2.8.3 pH of the solution ..... 13
2.8.4 Catalyst loading ..... 13
2.8.5 Surface Area and Morphology ..... 14
2.8.6 Effect of Light intensity ..... 14
2.9 Techniques to enhance photocatalitic efficiency ..... 15
2.9.1 Doping ..... 15
2.9.2 Composite formation ..... 18
2.9.3 ZnSe based composites for photocatalytic activity ..... 19
2.9.3.1 ZnSe/ZnTe ..... 19
2.9.3.2 ZnSe/TiO2 ..... 19
2.9.3.3 ZnSe/ Graphene ..... 20
2.9.3.4 ZnO/ZnSe ..... 20
2.10 Synthesis Methods for Photocatalytic Materials ..... 22
2.10.1 Sol- gel method ..... 22
2.10.2 Hydrothermal and solvotermal method ..... 22
Chapter 3 ..... 23
3.1 Materials and methods ..... 23
3.2 Characterization Instruments ..... 23
3.3 Experimental Design ..... 24
3.3.1 Synthesis of ZnSe ..... 24

3.3.2 Synthesis of $Co_2SiO_4$ ..... 25
3.3.3 Synthesis of $ZnSe/Co_2SiO_4$ ..... 26
3.4 Photocatalytic Dye Degradation Test ..... 27
Chapter 4 ..... 28
Result and discussion ..... 28
4.1 XRD results ..... 28
4.2 TGA-DTA analysis ..... 30
4.3 Optical property (DRS results) ..... 33
4.4 Morphological Analysis ..... 34
4.5 Photoluminescence spectra analysis ..... 35
4.6 FTIR results ..... 36
4.7 Photocatalytic Dye Degradation activity ..... 37
4.7.1 Images of Degraded methylene blue ..... 41
4.8 Recyclability Test ..... 43
4.9 Possible Photocatalytic Mechanism ..... 44
5 Conclusion ..... 45
Reference ..... 46

# List of Figures

Figure 2. 1 Mechanisms of photocatalytic dye degradation .....7
Figure 2. 2 Electron–hole separations on a heterojunction photocatalyst .....8
Figure 2. 3 Types of Semiconductor Hetrojunction .....9

Figure 3. 1 Schematic illustration for Synthesis of ZnSe .....24
Figure 3. 2 Schematic illustrations for Synthesis of $Co_2SiO_4$ .....25
Figure 3. 3 Schematic illustrations for Synthesis of $Co_2SiO_4$ .....26

Figure 4. 1 X-Ray diffraction of as prepared ZnSe .....28
Figure 4. 2 X-Ray diffraction of as prepared $Co_2SiO_4$ .....29
Figure 4. 3 the DTG-TGA curve for $Co_2SiO_4$ Prepared from sodium silicate as a silicate sour..
.....30
Figure 4. 4 XRD of a) $Co_2SiO_4$ (annealed at 800$^oC$ for 3h), and b-d) ZnSe/$Co_2SiO_4$ composites……..31

Figure 4. 5 kubelka plot of synthesized a) ZnSe, b )$Co_2SiO_4$ and c-d) ZnSe/ $Co_2SiO_4$ Composite .....33
Figure 4. 6 SEM images of a) ZnSe, b) $Co_2SiO_4$, c) ZnSe/$Co_2SiO_4$ .....34
Figure 4. 7 PL of a) ZnSe, b) $Co_2SiO_4$ and c) ZnSe/$Co_2SiO_4$ (60/40) .....35
Figure 4. 8 FTIR of a) ZnSe, b) ZnSe/$Co_2SiO_4$ and c) $Co_2SiO_4$.....36
Figure 4. 9 The visible light absorption spectra of methylene blue (MB) observed at regular time intervals, with the (a) ZnSe, (b) $Co_2SiO_4$, (c) ZnSe/$Co_2SiO_4$ (80/20), d) ZnSe/$Co_2SiO_4$(70/30, e) ZnSe/$Co_2SiO_4$(60/40)samples and f) $C/C_0$ photocatalytic degradation rates of ) ZnSe, $Co_2SiO_4$ and ZnSe/ $Co_2SiO_4$ composites……..38

Figure 4. 10A) % degradation of methylene blue (MB) observed at regular time intervals, with the ZnSe, $Co_2SiO_4$ and ZnSe/ $Co_2SiO_{4\,(60/40)}$ samples B) ln($C_0$/C) versus irradiation time for different photocatalysts……..……39

Figure 4.11 Images of degraded methylene blue…….....41

Figure 4. 12 Recycling experiments for the degradation of MB using ZnSe/$Co_2SiO_4$ (60/40) as photocatalys……...43

Figure 4.13 Proposed photocatalytic dye degradation mechanis…….....44

# List of Tables

Table 2. 1 Summary of ZnSe based composite .....21

Table 4. 1 Average crystal size of samples .....32

Table 4. 2 degradation efficiency of samples with respective irradiation time .....40

Table 4. 3 The pseudo-first order rate constant (k) and Average value of $C/C_0$ of samples .....42

# List of acronym and symbols

| | |
|---|---|
| CB | Conduction band |
| DRS | Diffused Reflectance Spectroscopy |
| $E_g$ | Energy bandgap |
| FTIR | Fourier Transform Infrared spectroscopy |
| Hr. | Hour |
| hv | Photon energy |
| $HO_2$ | Per hydroxyl radical |
| MB | Methylene Blue |
| $O_2^{\cdot}$ | Superoxide radical |
| OH | Hydroxyl radical |
| PL | Photoluminescence |
| QD | Quantem Dote |
| SEM | Scanning Electron Microscop |
| TGA-DTA | ThermogravimetricAnalysis-Differential Thermal Analysis |
| VB | Valence band |
| UV | Ultraviolet |
| UV-Vis | Ultraviolet Visible |
| XRD | X-ray diffraction |
| ℃ | Degree centigrade |
| ν | Frequency |
| θ | half Diffraction angle |

# Abstract

At present, photocatalysis technology based on semiconductor photocatalysts has been proven to be efficient method in dye wastewater treatment. It is the most promising and cost-effective approaches to reduce environmental hazards significantly related to the industrial development. In this research, ZnSe, $Co_2SiO_4$ and their composite ZnSe/$Co_2SiO_4$ photocatlytic semiconductor were successfully synthesized by solvothermal and sol-gel method, respectively. The X-ray diffraction, UV–Vis diffuse reflectance spectroscopy (DRS), Photoluminescence (PL), Fourier transform Infrared (FT-IR) and scanning electron microscope (SEM) were used for characterization of the synthesized sample.

The photocatalytic activity of ZnSe, $Co_2SiO_4$ and their composite ZnSe/$Co_2SiO_4$ were evaluated for degradation of Methylene blue (MB) dye under visible light irradiation. The results show that, the degradation potential of bare ZnSe and $Co_2SiO_4$ after 75min irradiation was about 37.7% and 30.5% respectively. However, the degradation potential of ZnSe/$Co_2SiO_4$ (80/20), ZnSe/$Co_2SiO_4$ (70/30), ZnSe/$Co_2SiO_4$ (60/40) composite after 75min irradiation time are 93.6%, 94.3%, 96.6% respectively. Compared with pure ZnSe and $Co_2SiO_4$, the ZnSe/$Co_2SiO_4$ Composite exhibited excellent photocatalytic performance for the degradation of methyl Blue dye, which was attributed to the effective separation of electron–hole pairs and improved light absorption result from coupling of ZnSe and $Co_2SiO_4$. Among the three synthesized composites, ZnSe/$Co_2SiO_4$ (60/40) show better photocatlytic degradation performance indicating that the molar ratio of ZnSe to $Co_2SiO_4$ plays an important role in determining photocatalytic activity. Furthermore, the photocatalytic activity of the composite photocatalyst was retained after four recycling runs and the result shows that the composite has high stability under visible light irradiation.

# Chapter One

# Introduction

## 1.1 Background

Water pollution caused by hazardous organic chemicals used in industry and agriculture is a very serious problem[1]. The industrial revolution has led to the pollution of the natural resources in massive proportions. Environmental pollution caused by anthropogenic sources is a day-to-day problem faced by both developing and developed countries. Both air and water pollution contributes a major share of the overall imbalance of the ecosystem. Wastes released from textile industries contains large amount of dangerous organic pollutants and heavy metals which contain serious environmental problems because of their harmfulness, potential carcinogenicity and non-biodegradability[2-3].

Common pollutants are usually toxic organic compounds like chlorinated and non-chlorinated aliphatic and aromatic compounds, dyes, detergents and surfactants, agro wastes like insecticides, pesticides and herbicides, disinfection byproducts, volatile organic compounds, plastics, inorganic compounds, noxious gases and pathogens[4]. Clean and non-polluted water is one of the basic requirements for all living organisms including human beings. But its availability is a major issue nowadays. Pesticides have a great contribution in the production of vegetable, fruit, cereal, fiber, forage, and oil crops, and their rate of consumption have been considerably increased.[5]. But when these pesticides have been used inappropriate way, they may cause for the pollution of food chain, soil, water and air[6]. Sraw at el. reported that they can be taken as the second-largest pollutant in the drinking water[7]. Moreover, although they are in small amount they can damage nerve and endocrine system of human body[8].

In the future, this issue will further increase due to global industrialization and population growth. Natural water is being contaminated by the discharge of industrial, domestic, and agricultural wastes[9]. The use of dyes in paper, plastics and textile industries has caused an increase in environmental pollution due to the amount of wastewater containing dye stuffs that are discharged into aquatic systems[2,15].

Dye wastewater mainly contains organic pollutants and toxic substances, which are difficult to be biodegraded. At present, photocatalysis technology based on semiconductor photocatalysts has been proven to be an inexpensive and efficient method in dye wastewater treatment. Due to their catalytic properties of low cost, low energy consumption and has no secondary pollution, Semiconductor photocatalytic technology has gotten a great attention[11-12].this process is a green technology which require visible light active semiconductor[13].

Among several methods used for removing toxic substances from industrial wastewater, Photocatalytic materials are good materials for purification of waste waters[14]. Indeed, photocatalytic process is the simplest and cost-effective process for removing organic and inorganic pollutions from the waste waters[15]**.** also heterogeneous photocatalysis has been studied as an emerging and efficient technique[16]. Recent studies have shown that heterogeneous semiconductor ($TiO_2$ and ZnO) photocatalysis can be an alternative to conventional methods for the removal of dye pollutants from water. ZnO and $TiO_2$ are the two most important photocatalytic materials due to their stability during the photocatalytic process. But, these two photocatalytic materials have wide band-gap value, which is disadvantage for photocatalytic activity. So that, they cannot be applicable under a visible-light source irradiation[18]. The photocatalysis technique is based on the illumination of semiconductor particles, usually suspended in aqueous solutions. The illumination of these particles with light energy greater than the band gap energy leads to the production of high energy electron–hole pairs, which can migrate to the surface of the photocatalyst and can either recombine producing thermal energy or participate in redox reactions with the compounds that are adsorbed on the photocatalyst's surface, thus, leading to complete mineralization of the organic compounds[19].when these semiconductors are illuminated with an appropriate light source, the electron/hole pairs are produced with electrons promoted to the conduction band and leaving the positive holes in the valence band. The generated electron/hole pairs induce a complex series of reactions that might result in the complete degradation of the dye pollutants adsorbed on the semiconductor surface[20].

Therefore, absorption of light, formation of photogenerated electron-hole pairs, transfer of electrons and holes, and occurrence of catalytic reaction are the main factors that should be considered during synthesis of photocatalytic semiconductor[21-22].

## 1.2 statement of the problem

The photocatalytic activities of ZnSe semiconductor, particularly nanostructures, have gotten much consideration. Researches show that ZnSe structures can only reveal their great photocatalytic activities under UV light irradiation, in spite of the fact that they have the absorbing edge for visible light. Zhang et al. investigated the photocatalytic activity of ZnSe flowerlike hierarchical structures for the degradation of methyl orange (Moment) dye under visible light. But MO dye totally removes after irradiating for about 9h this show us their efficiency is so low.

In addition to the efficiency problem (under visible light), this semiconductor during photocatalytic activity reacts with pollutants and so it cannot be utilized for several times in photocatalytic activity [34]. Consequently, it ought to be protected by another material that can be participated within the photocatalytic process. The other issue is short life span of photogenerated electrons-hole pairs which in turn limit their practical realization. During photocatalysis process the recombination of electron-hole pairs are major factor which determine photocatalytic activity[22]. In order to enhance photocatalaytic activity of the semiconductor material the recombination of charge carriers must be controlled.

Several methodologies are employed within the past to reduce the electron–hole recombination. However, in this research we use heterostructure formation to improve the activity of photocatalytic material. Formation of heterojunction structure is one the most excellent semiconductor-semiconductor junctions for the photocatalytic activity with high efficiency[21,23].

Semiconductors composites (hetrostructurs) have been proved to extend strongly the absorption rang and improve the absorption of the solar spectrum. Not only this, but also when it compared with a single semiconductor, semiconductors composites(hetrostructurs) promote the generation and separation of photo-induced electrons and holes, so that they can greatly enhance the photocatalytic efficiency[22-26].

## 1.3 General Objective

To design and synthesize efficient ZnSe/$Co_2SiO_4$ composite for effective removal of methylene blue (MB) dye in water.

### 1.3.1 Specific Objective

- ✓ To synthesize ZnSe with hydrothermal method and study the morphology, optical & Crystallography properties.
- ✓ To synthesize $Co_2SiO_4$ in sol-gel method, study the morphology, optical & Crystallography properties.
- ✓ To synthesize ZnSe/ $Co_2SiO_4$ Composite.
- ✓ Measure potocatlytic performance of ZnSe, $Co_2SiO_4$, ZnSe/$Co_2SiO_4$ composite.

### 13.2 Significance of the study

Significance of this study is synthesizing and characterize ZnSe/$Co_2SiO_4$ composite for the degradation of MB dye from waste water. Due to its high performance and low cost, it is applicable for textile industries to treat waste water which is contaminated by organic pollutants released during the industrial processing. On the other hand, human life, plants and animals which suffer from water contamination will be primarily beneficial from this research.

# Chapter 2

# Literature Review

## 2.1 Water Pollution

Water is an essential element for all human being living on the earth, and it is considered as the most precious resource of human civilization. The depletion of available water resources is attracting more and more attention around the world due to its key role in socio-economic development and human health. This is due to excessive use of water and increasing water pollution. Due to the diversity of manufactured products and the diversity of related chemical precursors which can be discharged into water resources, the industrial wastewater pollution has become a serious and complex problem[27-28].

Recently, the growth of industrial and agricultural activities has made it the main responsibility for the continuous discharge of toxic organic pollutants into water bodies without any treatment.[29-30]. These industries are considered to be the main sources of hazardous pollutants in the environment[31]. Azo dyes are mainly used pollutants because of their dangerousness, they are considered to be the most harmful type of organic pollutants[31].

Many substances such as heavy metals, dyes, surfactants, water-soluble organic pollutants, pharmaceuticals, pesticides, personal care products and many other substances can pollute water resources[32-33]. Organic, inorganic or microbial substances can also contaminate water, but they can be removed by adsorption[34], electrochemical processes[35], bioremediation and in oxidation processes[36]. Continuous and stable supply of energy is considered as one of the most challenging tasks to fulfill the energy demands due to rising population and enhanced living standard[37].

Sunlight is an inexpensive, non-polluting, abundant and endlessly renewable source of clean energy. The amount of energy that strikes the Earth yearly in the form of sunlight is approximately ten thousand times the total energy that is consumed on this planet, so converting solar energy into an easily usable form has attracted considerable interest in the last several decades[38].

Due to the potential of utilizing freely available solar energy for environmental remediation and fuel generation, Elimination of organic dyes using photocatalysis process has been attracting increasing attention in recent years[39- 41].

However, high amounts of effort have been performed for the decontamination of waste waters with the aid of UV light active photocatalysts. Due to the low amount of UV light in the solar spectrum, this idea is not very suitable in industrial application [42]. Hence, visible light photocatalysis can be a promising option for the effective use of solar spectrum[41]. This process needs enough amount of visible light to start its photocatlitic activity so that the amount of visible light irradiation is important prerequisite for the waste water treatment. Always the photocatalyst with a high activity and efficient response to visible-light irradiation are highly desirable[43].

Among different semiconductor photocatalysts, ZnS[44-45], ZnO,[17-46] and $TiO_2$[47,16,7] are attracting a great deal of research interest for photocat alysts. However, since they have relatively wide band gaps they can only be excited under ultraviolet light irradiation, which greatly limit theirs practical application in photocatalysis process. Usually, doping is a common way to reduce the band-gap value of these wide band-gap semiconductors and to create defect energy levels in the band gap space Which leds to absorb the visible light photons[15]. In the total sunlight the ultraviolet light accounts for only 3–5%, but visible light accounts 44–47%[48-49].

## 2.2 Methods of Wastewater Treatment

There are numerous methods which have been established for the elimination of organic pollutants from the waste water, among those some are like physical adsorption, anaerobic treatment, membrane filtration, chemical oxidation, biological method, and photocatalytic degradation method. Due to it uses solar energy for environmental purification, photocatalytic dgradetion has gotten much more attrition[29,22]. Photocatalysis process based on semiconductors has received great attention because it can degrade different organic pollutants into harmless yields (such as $CO_2$, $H_2O$, etc.)[50]. There are different kinds of methods to remove pollutants from aqueous environment such as adsorption, advanced oxidation processes, nano filtration, electro-coagulation and biological de- gradation [4].

## 2.3 Mechanism of photocatalysis dye degradation

Mechanism of photocatalysis dye degradation is based on generation of electron–hole pairs in semiconductor materials when photon energy greater than or equal to the band gap is absorbed, inducing excitation of electrons from valance band to the conduction band[51]. these electron–hole pairs can further produce free radicals and provide redox reactions of compounds absorbed on the surface of the photocatalyst. The consequential free radicals, like hydroxyls (OH), are very good for the degradation of organic pollutants[52].

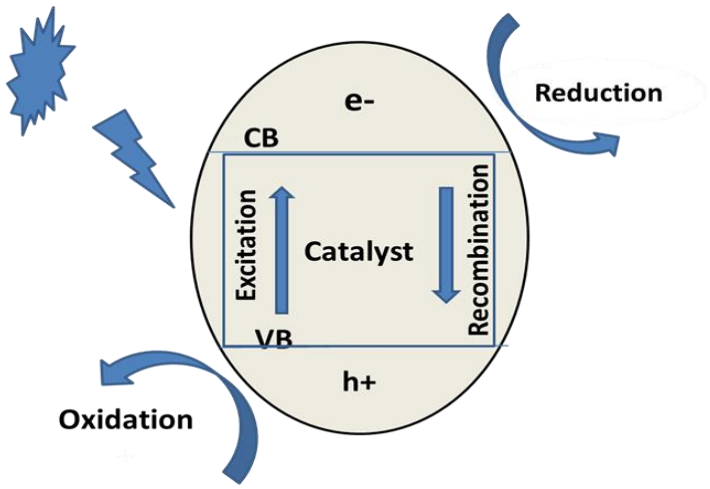


*Figure 2. 1 Mechanisms of photocatalytic dye degradatio*

As shown in the above Figure 2.1, when semiconductors are irradiated with energy higher than their band gap, electron and hole pairs are generated. It results in the excitation of an electron from valance band to conduction band, leaving a positive hole behind (hVB+). The hVB+ and eCB- are strong oxidizing and reducing agents, respectively[53]. The hVB+ reacting with water to generate •OH. The hydroxyl radical (•OH) produced by has the second-highest oxidation potential (2.80 V). Owing to its electrophilic property, the •OH can generally oxidize almost all electron rich organic molecules, finally converting them to $CO_2$ and water. The electrons in the conductive band can react with $O_2$, resulting in an anion radical superoxide. Further reaction can lead to the creation of hydrogen peroxide that lead to the creation of •OH. Dissolved oxygen is extremely important to limit recombination which is very essential for photocatalytic degradation[54,55,40].

## 2.4 Semiconductor Heterojunction photocatalysts

A heterojunction, in general, is defined as the interface between two different semiconductors with unequal band structure, which can result in band alignments[22]. This type of photocatalysis based on semiconductors has received great attention due to its potential in solving environmental problems. For instance, ZnO/ZnSe[58,30,59,60,61], ZnO/ZnTe[62,63], ZnS/ZnSe[3], ZnO/ZnS[25,64], ZnTe/ZnSe[31] have great role for degradation of organic pollutants in waste water. This technique is based on electron-hole generation by irradiation with suitable energy light of semiconductor materials. Nanosized particles have distinctive physical and chemical properties from the bulk that make them applicable in the photocatalytic process. The photocatalytic degradation of hazardous compounds (dyes, pesticides, etc.) in an aqueous medium depends on the band gap, surface area, amount of catalyst, etc. Different metal oxides and sulfides have been working as photocatalysts for photodegradation of dyes[23]. The separation of photogenerated electron–hole pairs on the surface of a photocatalyst is very difficult to achieve. Although preventing electron–hole recombination is a very challenging task, it can be accomplished by the proper design of a photocatalyst. Various strategies have been proposed to efficiently separate the photogenerated electron–hole pairs in semiconductor photocatalysts, for instance by doping[65], metal loading[66], and/or introducing heterojunctions[67]. Among the proposed strategies, engineering heterojunctions in photocatalysts has been proved to be one of the best method for the preparation of advanced photocatalysts,( see Figure 2.2)[22].

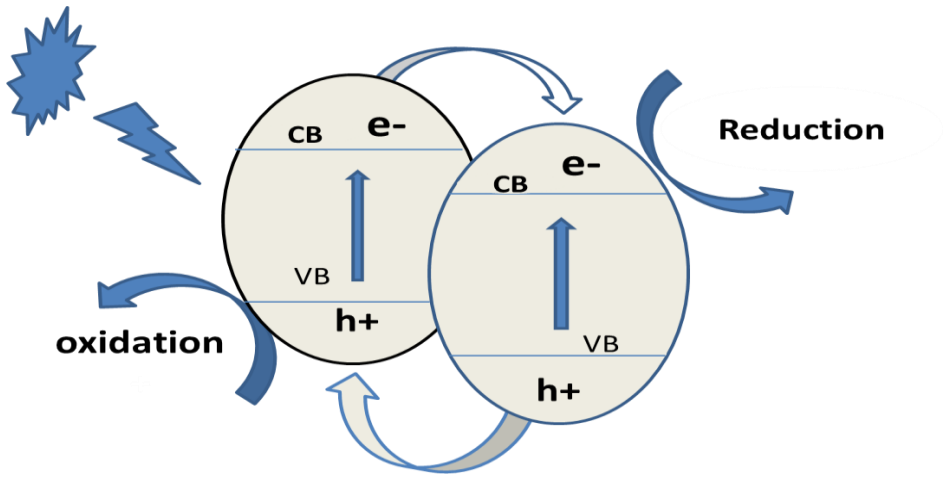


*Figure 2. 2 Electron–hole separations on a heterojunction photocatalyst*

Basically, there are five different types of heterojunctions, these are conventional type-II heterojunctions[68-69], p–n heterojunctions[70-72]. surface heterojunctions[73-75] direct Z-scheme heterojunctions[76-77], and semiconductor–graphene (SC–grapheme heterojunctions[78,47].

### 2.4.1 Conventional hetrojunction

There are three types of conventional hetero- junction photocatalysts, which are characterized, based on their straddling gap, type-I, type-II, and type-II, see fig 2.3 below. In case of type-I het- erojunction photocatalyst, the conduction band (CB) and the valence band (VB) of semiconductor are respectively higher and lower than the corresponding bands of semiconductors[79]. Therefore, under light irradition, the electrons and holes will accumulate at the CB and the VB levels of semiconductor B, respectively. Since both electrons and holes accumulate on the same semiconductor, the elec- tron–hole pairs cannot be effectively separated for the type-I heterojunction photocatalyst[22].When a heterostructure is used in a photocatalytic reaction, type II is usually the most common, because this heterostructure can effectively promote charge transfer and extend the life of charge carriers[37].

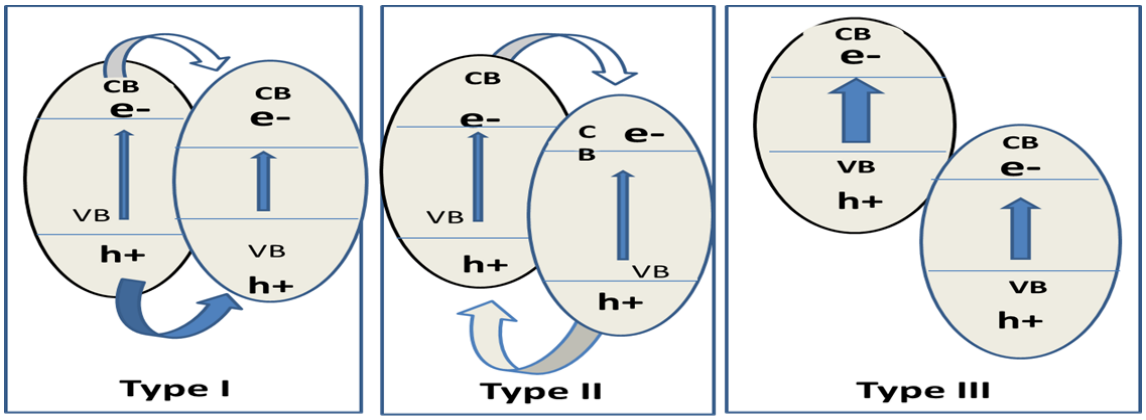


*Figure 2. 3 Types of Semiconductor Hetrojunction*

In this type of heterojunction, the energy gradient at the interface tends to separate electrons and holes spatially on different sides of the heterojunction, the electrons are fixed on one side and the other side occupied by holes.

Type II should make these materials more suitable For photocatalytic applications. Such semiconductor heterostructures can easily integrate small and wide bandgap materials to drive water oxidation/reduction processes simultaneously via multiple combinations[79]. Various attempts have been made in the past to obtain type II heterojunctions, such as; $TiO_2/g\text{-}C_3N_4$ [37], $BiVO_4/WO_3$[80], $AgI/Bi_7O_9I_3$ [81], $C_3N_4$– $BiPO_4$ [82].

As shown in Figure 2.3, the structure of the type III heterojunction photocatalyst is similar to that of the type II heterojunction photocatalyst, beside that the gap becomes so large that the band gaps do not overlap. Two semiconductors cannot be used in type III heterojunctions, making them unsuitable for improving the separation of electron-hole pairs.

## 2.5 Photocatalytic Semiconductors

Photocatalytic semicondctors are essential substances for purification of waste water. In fact, the photocatalytic process of semiconductor nanostructures is the simplest and most economical process to remove organic and inorganic pollutants in water. Therefore, various semiconductor nanostructures such as ZnO, $TiO_2$, CuO, AgX (Br and Cl) and $Ag_2CO_3$ are used as photocatalytic Materials in the past few decades.[15] and they can be divided into two types: (i) homogeneous photocatalysis, (ii) heterogeneous photocatalysis[83].

Titanium dioxide ($TiO_2$) is undoubtedly the most widely used photocatalyst due to its biological and chemical stability, non-toxicity, cost-effectiveness and high activity.however, Due to its large band gap (3.2 eV), it can only use ultraviolet light, so it can only use 3-5% of the total solar radiation reaching the earth at the ultraviolet frequency[18].

Different well-structured semiconducting metal oxides such as $TiO_2$, porous ZnO films, anatase $TiO_2$ nanoparticles, well- aligned single-crystalline ZnO nanobelt arrays fabricated on a Si wafer and ZnO powders with various size scales were prepared and their catalytic performance were tested for the degradation of MO under UV illumination[8]**.**

Due to their potential application in nano device various studies have been conducted on II–VI chalcogenide semiconductor materials, such as ZnS[40,84], CdS[85- 87], ZnSe[18,43,88,89], CdSe[90-91], CdTe[92-93] and ZnTe[94], Unique energy band gap characteristic of these semiconductor materials is one of the most important properties[95].

## 2.6 Photocatalitic property of ZnSe

Among various semiconductors which used for photocatalytic materials, zinc selenide semiconductors is a promising candidate due to its suitable band-gap (2.67 eV) in visible region. Such of its suitable band gap caused to report several works related to the photocatalytic performance of ZnSe nanostructures under visible region[96,15,18,60,88]. It is found that the ZnSe exhibit enhanced photocatalytic activities for the degradation of MO dye under UV light or visible light[88].

However, this semiconductor during photocatalytic activity reacts with pollutants and so it cannot be utilized for several times in photocatalytic activity [34]. Consequently, it should be protected by another material that can be participated within the photocatalytic process. The other issue is short life span of photogenerated electrons-hole pairs which in turn limit their practical realization. During photocatalysis process the recombination of electron-hole pairs are major factor which determine photocatalytic activity[22]. In this research we investigate the photocatalitic activity of ZnSe, $Co_2SiO_4$ and their composite (ZnSe/$Co_2SiO_4$).

## 2.7 Photocatalitic property of Co2SiO4

The $Co_2SiO_4$ nanostructures show a good degradation performance due to its high potential to be applied as a novel, and effective type of photocatalyst under UV light irradiation for degradation of the organic dyes. It can be applicable for photocatalytic activity of three (Methyl orange, methylene blue, erythrosine) pollutants under UV light[97]. Also it has good photocatalytic efficiency under UV light irradiation for acid black, acid brown and methyl orange[98].

## 2.8 Parameters affecting photocatalytic activity

### 2.8.1 Calcination temperature

The calcination temperature is an important parameter in the synthesis of ceramic materials and catalysts and can play a critical role in controlling the physicochemical properties[99].Calcination is a treatment used to increase the photocatalytic activities, even though it is far from clear how it affects the physicochemical parameters that control the photoactivity[100]. it affects crystal phase, morphology and photocatalytic performance of the composites [11].

In general, an increase in the temperature of calcination provides a high crystallinity, a decrease in the surface area and, for mixed materials or doped semiconductors, an absorption shift toward the visible spectrum[101-104]. Various studies have been conducted on this area, and they confirm the great role of calcination temperature on photocatalyitic activity of semiconductor materials such as, $TiO_2$[99,105,106,107], $CuNi/TiO_2$[108], BiOX (X=Cl, Br)[109], $Ag_3PO_4$[109] $Bi_2Mo_6$ [110].

### 2.8.2 Concentration and nature of pollutants

Pollutants are depend on their nature, concentration and existence of other compounds to be degraded in photocatalytic materials. Not only the concentration but also the chemical structures of the target compound affect the degradation performance of the photocatalytic reactor. When the concentration of a dye solution increase, the photons get intercepted before they can reach the catalyst surface, so that this decreases the absorption of photons by the catalyst.[111]. Therefore, rate of degradation decrease with increasing concentration of dyes. [112].

### 2.8.3 pH of the solution

West water treatment based on potocatalytic material is significantly depending on the pH. Because it affects the charge on the catalyst particles, size of aggregates and the position of valance band and conduction band. This influence of pH made it attractive to be extensively studied[54]. Because of the amphoteric behavior of most semiconductor oxides, the pH of solution is important parameters that govern the rate of reaction taking place on semiconductor particle surfaces. Therefore, the effect of pH on the rate of degradation needs to be considered[111]. Several researches have been studied in this area, for instance $TiO_2$[4,113,114].

### 2.8.4 Catalyst loading

The concentration of catalyst in photocatalytic activity is one of the key parameters that control the degradation rate of the organic compounds. Concentration of catalyst is one of the mast significant parameters that govern the rat of degradation. And it is known thatdegradation rat of dyes and pollutants incrase with increasing load of catalyst[53,115].

At high photocatalyst concentration, the probability of particles to be agglomerated is high, which results in the reduction of the available surface area for the light intake and so that it reduces the generation of photoexcited electrons and holes which affects the photoactivity and reaction rate drops significantly[116,111]. many researchers have been studied on the influence of catalytic loading such as, $TiO_2$[4,53,114,117,118].

### 2.8.5 Surface Area and Morphology

photocatalytic activity of semiconductor materials can be affected by surface area, crystal composition, distribution, porosity, bandgap, particle size, and surface hydroxyl group density[100,116,119]. morphology also affect the photocatalytic property of the material[43,120]. Generally the degradation performance of the photocatalytic material is influenced by surface area and morphology. As a result, the dependency of the pollutant degradation rate on the surface area and morphology has been investigated in numerous studies using different pollutants, such as, $TiO_2$[121-122],tungsten–nitrogen-codoped titania[123].

### 2.8.6 Effect of Light intensity

UV irradiation generates photons essential for the electron to be exited from the valence band to the conduction band. The energy of a photon is related to its wavelength and the total energy required for photocatalytic process is dependent on the light intensity. So that, the influence of intensity and wavelength parameters are important[111]. The degradation efficiency of photocatalyitc semiconductor increase as a function of light intensity, whatsoever the photocatalytic conditions is[124]. the photocatalysis reaction was more efficient under more intensive light irradiation since more electron-hole pairs are activated, therefore the irradiation light can affect the reaction efficiency[112,125].

## 2.9 Techniques to enhance photocatalitic efficiency

Photocatalytic activity of semiconductors need improvement when the recombination rat is high[126]. Various approaches have been conducted to solve this issue such as;

### 2.9.1 Doping

Usually doping is a process of introducing metal or non-metal atoms in the host atom to increase the photocatalytic activity of a semiconductor without giving rise to a new crystallographic forms, phases or structures[127]**.**

Efficiency of a photocatalyst materials are highly influenced by its band structure. But, modifying the band gap of the photocatylitic material, so that it can work under visible light, is the request of noble photocatalysts. The band gap can be modified either by announcing a new band between the VB and CB or by strong interface interaction. This can be achieved by doping with a metal ion, a non-metal substance, covalent and non-covalent doping, etc. It is known that wide band gap semiconductors limit the light absorption of photocatalyst under UV region, that leds to restrict the efficiency of semiconductors[128].

Doping is an effective method to extend the light absorption to the visible light region. There are various classification of doping, such as self-doping, nonmetal doping, transitional metal doping, and rare-earth metal doping. Usually, the doped ions form additional new energy levels in the band structure, which is important to trap electrons or holes to separate carriers from the bands, thus allowing more carriers to successfully diffuse to the surface[129].

In general, commonly used dopants in photocatalytic semiconductor materials can be classified as the metal cations and the non-metallic elements[83,130].

#### 2.9.1.1 Metal Cation Doping

Doping of semiconductors may result in point defects which introduce the levels or states near, above or below the valence and conduction bands. When the metal is incorporated in a lattice(it is doped in the form of metal ion), it produces a band or energy level in the forbidden energy area which helps the material able to absorb visible light.

Furthermore, the doped metal in the form of metal ion can change the equilibrium concentration of charge carriers by acting as an electron acceptor, which increases the total quantum efficiency of the photocatalytic activity[83].

commonly used metal cation dopants for semiconductors are mostly including transition metal ions, such as $Fe^{3+}$, $Co^{3+}$, $Mo^{5+}$, $Ru^{3+}$, $Ag^{+}$, $Cu^{2+}$, $Rb^{+}$, $Cr^{3+}$, $V^{4+}$, etc. most of the time, the redox energy states of those working metal cations fall within the band gap states of corresponding semiconductors. So that, doping of those metal ions will result in an intraband state near the CB or VB edge of a semiconductor. Therefore, the red shift in band gap absorption of a metal-cation-doped semiconductor is mainly contributed by the charge migration between the d electrons of the doped cations and the CB (or VB) of the corresponding semiconductors. In addition, the doped metal cations can act as an electron–hole trap, regulating the charge carrier equilibrium concentration. Even if some transition metal cations could offer new energy levels as electron donors or acceptors, and effectively improved the visible light absorption capacity of corresponding semiconductors, this method is also known to undergo from many disadvantages, such as bad thermal stability, significant increase in the carrier-recombination centers, and the high cost for an expensive facility[83,130].

### 2.9.1.2 Non-Metallic Anions Doping

On the other hand, doping the semiconductors with appropriate non-metallic anions has been verified to be a facile way to control the intrinsic electronic structure of semiconductors and can construct various heteroatomic surface structure, so that it can improve photocatalytic activity under visible light irradiation. In general, there are two important factors for controlling electronic stat of the dopant and the corresponding heteroatomic surface structure of the catalysts, which are chemical stets and locations.

According to the researches, three basic criteria should be satisfied in doping of a semiconductor: (i) formation of states in the band gap of corresponding semiconductors should be appeared with an enhanced visible light absorption capacity, (ii) minimum of CB including the doped states should be equal to the semiconductor's or higher that the $H_2/H_2O$ level, therefor the photoreduction can be conducted, and (iii) the states in the gap should adequately overlap with the band states of semiconductors to certify that photoexcited carriers can migrate to the surface of catalysts within their lifetime [83,130].

Due to the band gap narrowing and the shift of absorption edge, nonmetal elements having high ionization energies and electronegativity, such as nitrogen, carbon, boron, sulfur, fluorine, and chlorine, are capable strategy to improve the visible light photocatalytic activity[129].

### 2.9.2 Composite formation

Heterogeneous photocatalysis has received a great attention due to its ability in solving environmental problems [1]. This method is based on the generation of electron-hole pairs by irradiating suitable photon energy in photocatalytic semiconductor materials[23]. The most widely used heterojunction semiconductors are $TiO_2$-based photocatalysts and some limited non-TiO2 based systems. Commonly researched composites are $TiO_2$-based photocatalysts include $WO_3/TiO_2$, $MoO_3/TiO_2$, $ZrO_2/TiO_2$, $Fe_2O_3/TiO_2$, $ZnO/TiO_2$, $SnO_2/TiO_2$, $Cu_2O/TiO_2$, $Bi_2O_3/TiO_2$, $CdS/TiO_2$, $Bi_2S_3/TiO_2$, and so forth[131]. Construction of heterojunction composite is a method of increasing the charge separation and absorption towards visible light region. Increasing charge separation will reduce recombination resulting in more production of reactive oxidizing species so that this leads to improve degradation of organic pollutants [83]. Heterojunction between two semiconductors improve the departure of photo-generated electron-hole pairs. Therefore, it is important to enhance the photocatalytic activity of the semiconductors[132].

### 2.9.3 ZnSe based composites for photocatalytic activity

Semiconductor materials have attracted increasing interest in recent years because of the unique structure, stable chemical properties and high performance in devices. With special properties such as a direct band-gap and excellent photoelectrical characteristics, ZnSe based semiconductor are promising materials for applications in such fields as photocatalysts, light-emitting diodes, solar cells, photodetectors, and so on. However, in Table 2.1 we summarize photoctlytic performance ZnSe based composites.

#### 2.9.3.1 ZnSe/ZnTe

ZnTe is a p-type semiconductor having a direct band gap value of 2.2eV at 300 K and is a promising material owing to its wide range of applications in solar cells, blue–green LEDs, and in optoelectronic devices. The phtoctlytic activity of ZnSe can be improved by forming a composite with zinc telluride[31,133]. ZnTe is widely used in photocatalysis owing to its narrow bandgap. Many reports have been published on the enhanced photocatalytic activity of various materials that form a heterojunction with ZnTe[136,137]. photocatalytic reaction system with semiconductor nanoparticles such as $TiO_2$, $Fe_2O_3$, $SnO_2$, and $WO_3$ as the nano-catalyst has been experimented in the previous studies. Among this catalyst, chalcogenide quantum dots (QDs) such as ZnTe QDs has applied in the photocatalysis system due to high electrical conductivity[138].

#### 2.9.3.2 ZnSe/TiO2

$TiO_2$ is the other important photocatalytic semiconductor material for environmental applications because of its strong oxidizing and reducing ability, low cost and availability. However, like ZnO, $TiO_2$ also responds only to UV light due to its wide band gap, which restricts its applications[139]. Many attempts have been devoted to improving the visible light photocatalytic activity of $TiO_2$. Recent, studies have reported various methods of coupling $TiO_2$ to a narrow-band gap semiconductor to enhance the photocatalytic efficiency under visible light irradiation. Therefore, Coupling $TiO_2$ with ZnSe could enhance the electron-hole separation and increase the charge carrier lifetime, which improve the photocatalytic activity of $TiO_2$[140].

### 2.9.3.3 ZnSe/ Graphene

Nanostructured carbon materials (e.g. graphene) has emerged as high potential material and increasingly attracted attention, due to its specific properties, including excellent electron mobil ity, large specific surface area, flexible structure, high transparency and stability at room temperature. When used to modify other materials, graphene can retard the recombination of electron-electron hole pairs that are photochemically or electrochemically generated; thus, graphene can increase the transfer of photogenerated charges and further increase the catalytic activity[141]. these properties are important features when dealing with the preparation and use of grapheme based materials and, for this reason, the combination of ZnSe and graphene could be a good preference to achieve an improved charge separation processes. Thus far, many researchers have reported the graphene based semiconductor Nano-composites exhibits enhanced photocatalytic activity. Among graphene based semiconductor photocatalysts, graphene-based ZnSe Nano-composites were expected to provide improved photoctalytic activity and promote extraordinary properties under visible-light irradiation[142-144].

### 2.9.3.4 ZnO/ZnSe

ZnO, an important wide and direct band-gap semiconductor (3.37 eV for bulk ZnO), is generally accepted as a promising photocatalyst due to its low ease of preparation, high catalytic efficiency and environmental sustainability[145]. However, ZnO can primarily utilize UV light, which is about 4% of the total sunlight reaching the earth. Therefore, it hardly absorbs any visible light, accounting for about 43% of the solar spectrum, thus restricting its potential as a solar-driven photocatalyst[49]. Moreover, practical applications are still impeded by its poor photostability due to photoinduced dissolution in photocatalytic processes. Thus, the key to promote the ZnO-mediated photocatalytic degradation is to modify the ZnO surface with another material for higher solar energy utilization efficiency and to enhance the separation of photogenerated charges.

Coupling a narrow band gap semiconductor with ZnO is regarded as an efficient strategy to extend the photoabsorption capacity of ZnO to the visible range and to reduce the tendency towards charge recombination. Therefore, ZnSe, with a suitable band gap (2.67 eV), is a good material to extend the visible light absorption of ZnO by constructing composites[146].

*Table 2. 1 Summary of ZnSe based composite*

| **Types of catalyst** | **Catalytic loading** | **Dye concentration** | **Dyes** | **Time** | **Efficiency** | **Reference** |
|---|---|---|---|---|---|---|
| **ZnSe** | 1g/L | 5mg/L | Orange II | 60min | 20.23% | [147] |
| **ZnTe/ZnSe** | 0.1g/L | 80mL | CR Dye | 65min | 94% | [31] |
| **ZnS/ZnSe** (1:1) &(1:3) | 10mg/L | 10mL | MO | 60min | 91.8-95.8% | [3] |
| **CuSe/ZnSe** | 0.3g/L% | 100mL | MO,MB | 60-90min | 96-100% | [149] |
| **$Yb_{0.064}Zn_{0.96}Se$** | 1g/L | 5mg/L | Orange solution | 60min | 64.01% | [147] |
| **$Nd_{0.066}Zn_{0.94}Se$** | 100g/L | 5mg/L | Acid orang 7 | 120min | 84.20% | [148] |
| **ZnSe** | 0.5g/L | 100Ml | Rh-6G | 120min | 44% | [150] |
| **ZnSe/$TiO_2$** | 1g/L | MO | 10mg/L | 30min | 80% | [23] |
| **ZnO/ZnSe** | 1×1.5 cm | 5 mL of $10^{-5}$ M | RhB | 120min | 96.0% | [59] |
| **ZnO/ZnSe** | 100 mg | 75 ppm | Congo red | 40min | 90.89% | [30] |
| **ZnSe/$TiO_2$** | 100mg | 10 mg /L | MO | 120 min | 80% | [23] |
| **ZnSe/ Graphene** | 10 mg | 35 mg/L | MB | 6h | 99.1% | [29] |

## 2.10 Synthesis Methods for Photocatalytic Materials

### 2.10.1 Sol- gel method

Sol–gel method is a good method for synthesis of nanomaterials consisting of the preparation of a sol, successive gelation, and solvent removal. This process indicates chemical transformation from a liquid "sol" into a gelatinous network "gel" phase with subsequent post treatment and transition into solid oxide material[151].

It is the most widely used methods which used to get homogeneous mixture in molecular of metal ion; this leads to enhance the formation of particles in special properties. In this synthesis method doping can easily be performed during gelation process[152].

The Sol is obtained by either hydrolysis or polymerization reactions by adding suitable reagents in the precursor solution whereas; gelation process done through condensation of the sol or addition of polymers converts this sol to gel. This gel can be used to form materials of different types such as nanoparticles, xerogel, glass or ceramics depending upon the further processing steps involved[153].

### 2.10.2 Hydrothermal and solvotermal method

The term "hydrothermal/solvothermal process" is defined as doing a chemical reaction in sealed vessels in which the temperature of solvents near their critical points via heating simultaneously with autogenous pressures. The process called as "hydrothermal" when water is used as the solvent, and it is called "solvothermal process" when organics are used as a solvent [154]. This technique is helped by steel pressure vessels known as autoclaves. It may have Teflon liners under controlled temperature or pressure[152]. this apparatus used to growth the crystals and the nutrient supplied along with water[155]. Material synthesis through hydrothermal/solvothermal methods is a crystallization process directly from solutions that usually involve two steps: crystal nucleation and subsequent growth. By controlling processing variables, such as temperature, pH, reactant concentrations, and additives, the final products could be fabricated with desired particle sizes and morphologies[154,156].

# Chapter 3

## 3.1 Materials and methods

Solvothermal and sol-gel methods have been used to synthesize ZnSe and $Co_2SiO_4$ respectively, and the composite $ZnSe/Co_2SiO_4$ also formed via sol-gel method. Zinc acetate ($Zn(CH_3COO)_2$), Se powder, Sodium hydroxide(NaOH), sodium silicate($Na_2SiO_{3)}$ and cobalt nitrate($Co(NO_3)_2$) were used as precursors, whereas Ethylene glycol(EG) and distilled water were used as solvents. All the chemicals and reagents purchased from loba chemie PVT.LTD. All the experiments and characterizations have been done in materials science and engineering department, ASTU.

## 3.2 Characterization Instruments

All the synthesized samples are characterized by X-ray diffractometer (XRD), Scanning Electron Microscope (SEM), UV–Vis diffuse reflectance spectroscopy (DRS), UV-Vis spectroscopy, Photoreactor, Photoluminescence Spectroscopy and Fourier transform infrared (FT-IR).

## 3.3 Experimental Design

### 3.3.1 Synthesis of ZnSe

The ZnSe were synthesized by solvothermal method, both zinc acetate ($Zn(CH_3COO)_2$) and Se powder were used as Zn and Se source respectively. 10 mmol of Se powder was dissolved in 30 mL of NaOH solution (2mol/L). After stirring for 15 min, 10 mmol of zinc acetate was added into the solution and then stirred for 30 min. Finally, 20 ml of EG were poured into the above solution. After stirring 1h, the solution was transferred into an 80ml stainless steel Teflon lined autoclave. The autoclaves were sealed and heated at 180 ℃ for 24 h. when the reaction time end, the autoclave was then cooled to room temperature. The products were centrifuged and washed five times in distilled water and two times in ethanol. Finally, the products were dried in vacuum oven at 80 ℃ for 8 h to obtain yellow powder sample[18]. Figure 3.1 shows the solvothermal synthesis of ZnSe.

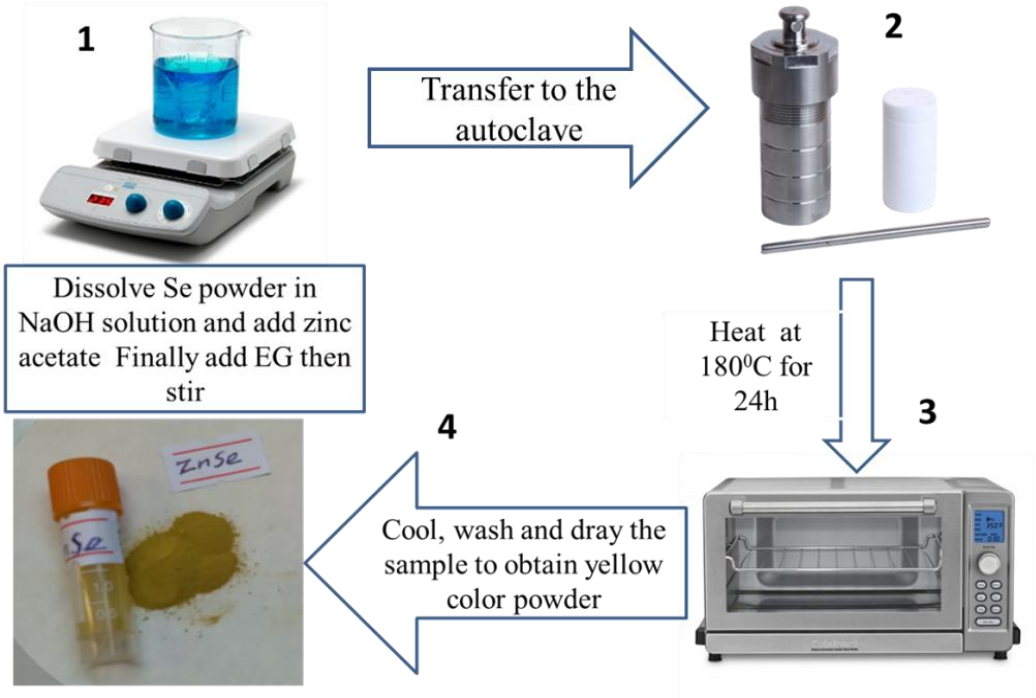


*Figure 3. 1 Schematic illustration for Synthesis of ZnSe*

### 3.3.2 Synthesis of $Co_2SiO_4$

The $Co_2SiO_4$ were synthesized by the sol–gel method, starting from cobalt nitrate and sodium silicate. The $Co_2SiO_4$ was prepared by slowly dropping 5ml of a 4M $Na_2SiO_3$ solution and 5 ml of a 2M $Co(NO_3)_2$ solutions into 40 ml water under rapid stirring. After 1h stirring, a viscose gel was obtained. The gel then washed 4times by distilled water and 2 times by ethanol and then dried in vacuum oven at 80°C for 8h and a bluish violet (purple) powder was obtained. The dried gel was calcined at 800°C for 3 h and a blue like powder was obtained[157]. Figure 3.2 shows synthesis of $Co_2SiO_4$.

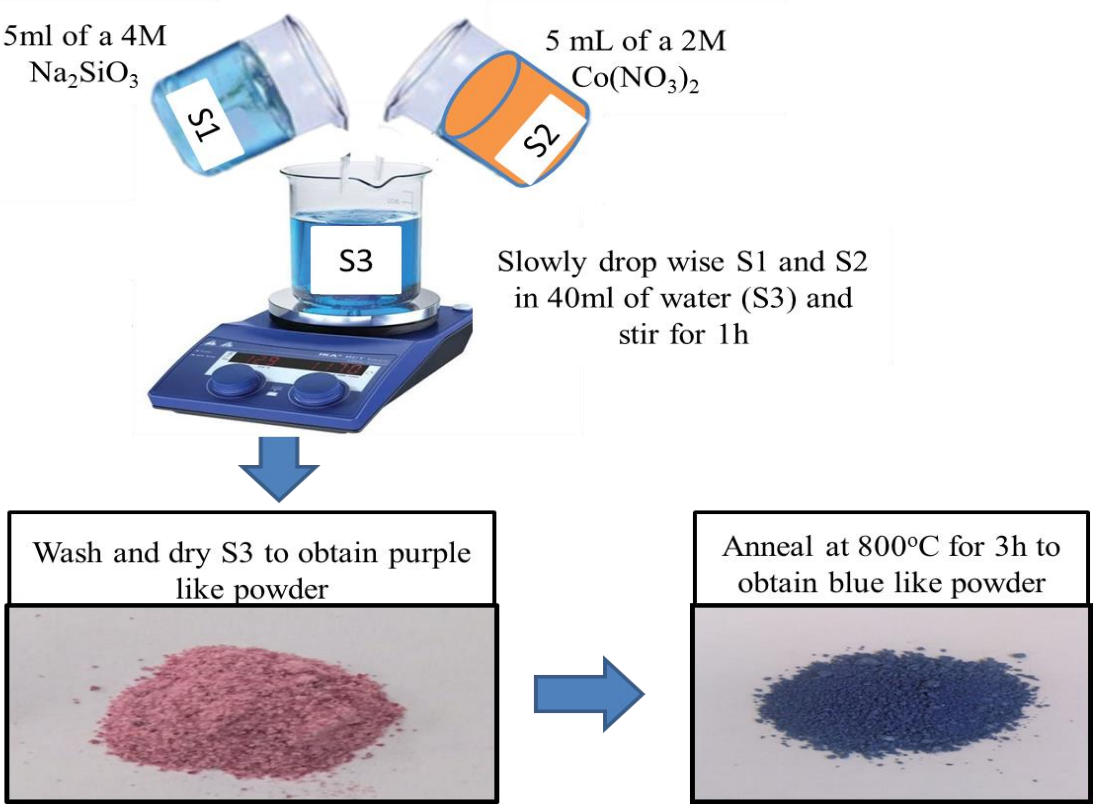


*Figure 3. 2 Schematic illustrations for Synthesis of $Co_2SiO_4$*

### 3.3.3 Synthesis of ZnSe/$Co_2SiO_4$

Three different molar ratio of ZnSe to $Co_2SiO_4$ composites have been synthesized by simple sol-gel technique such as, ZnSe/$Co_2SiO_4$(80%/20%), ZnSe/$Co_2SiO_4$(70%/30%), ZnSe/$Co_2SiO_4$ (60%/40%). The composite were synthesized by dissolving appropriate amount of ZnSe and $Co_2SiO_4$ in 20ml of ethylene glycol (EG) individually, and separately sonicated for 30min to be dispersed. After sonication, the two solutions have been mixed by drop wise. After stirring for 3h, the products were centrifuged and washed three times in distilled water and two times in ethanol. Finally, the products were dried in vacuum oven at 80 ℃ for 8h to obtain ZnSe/$Co_2SiO_4$. The corresponding products were denoted as 80/20, 70/30 and 60/40% percent of ZnSe to $Co_2SiO_4$, respectively. Figure 3.3 shows synthesis of composites.

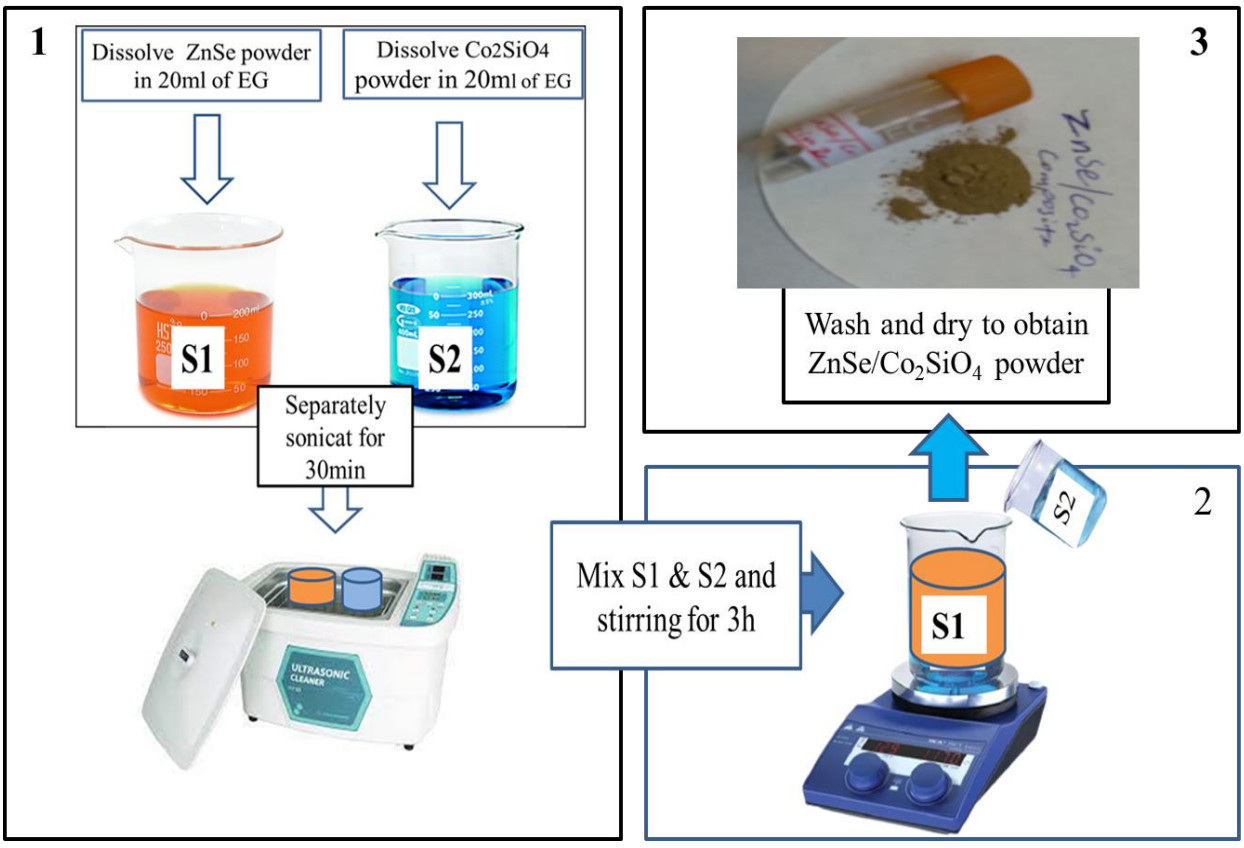


*Figure 3. 3 Schematic illustrations for Synthesis of $Co_2SiO_4$*

## 3.4 Photocatalytic Dye Degradation Test

The photocatalytic activities of the ZnSe, $Co_2SiO_4$, $ZnSe/Co_2SiO_4$(80/20), $ZnSe/Co_2SiO_4$(70/30), $ZnSe/Co_2SiO_4$(60/40) have been investigated for the degradation of Methyl Blue(MB) aqueous solutions under visible light irradiation. The irradiation was afforded by a 150W halogen lamp with a cutoff wavelength of 420 nm. 50 mg of each sample were used in 10 ppm of MB to investigate their photocatalytic activity. The samples were placed in the bottom of a cuvette containing 100ml of MB aqueous solutions (10 ppm). The photocatalytic tests of all samples have been done at room temperature. In every 15min irradiation time intervals, the solution concentration of MB have been taken and analyzed by a UV–Visible spectrometer.

# Chapter 4

# Result and discussion

## 4.1 XRD results

The XRD pattern of the synthesized ZnSe is shown in Figure 4.1. All the diffraction peaks of the samples are in good agreement with the given diffraction data of standard ZnSe(JCPDS file 000371463). According to the XRD pattern, the crystallinity of products is high and the planes of (111), (220), (311), (400) and (331) for ZnSe have been observed in the 2θ range value from 26 to 73°. All the peaks are arising from ZnSe, no other impurities were observed, indicating that the high purity of the sample and the final product were pure FCC ZnSe.

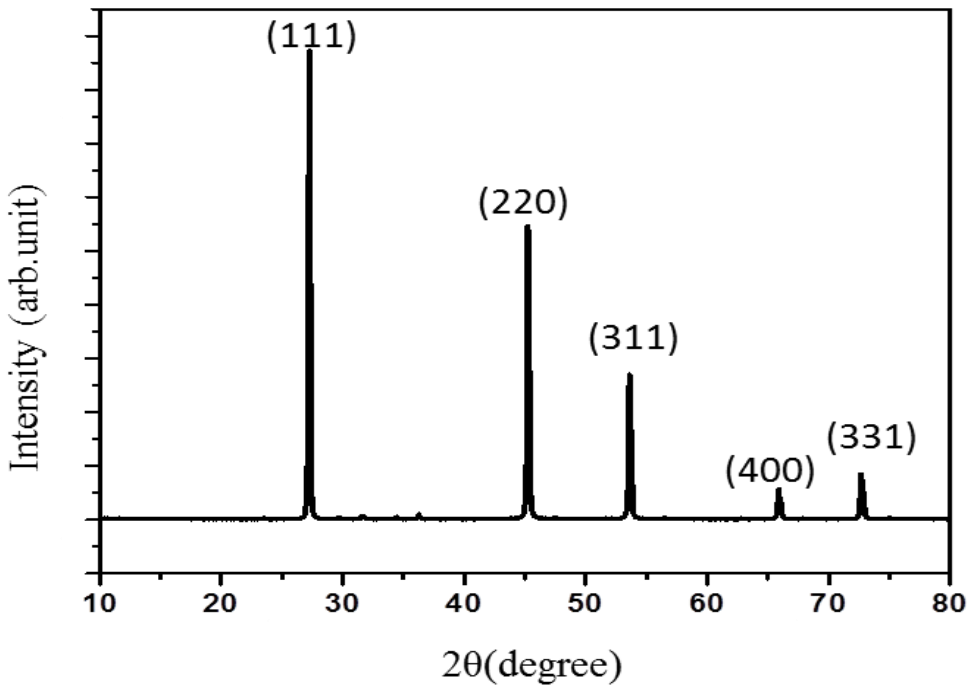


*Figure 4.1 X-Ray diffraction of as prepared ZnSe*

The XRD pattern of the as synthesized $Co_2SiO_4$ is shown in Figure 4.2, which doesn't have diffraction peaks, confirming its amorphous nature, whereas Figure 4.3 shows the DTG-TGA curve of $Co_2SiO_4$. As shown in the red curve in Figure 4.3 the $Co_2SiO_4$ powders become stable in the temperature range between 700- 900c.

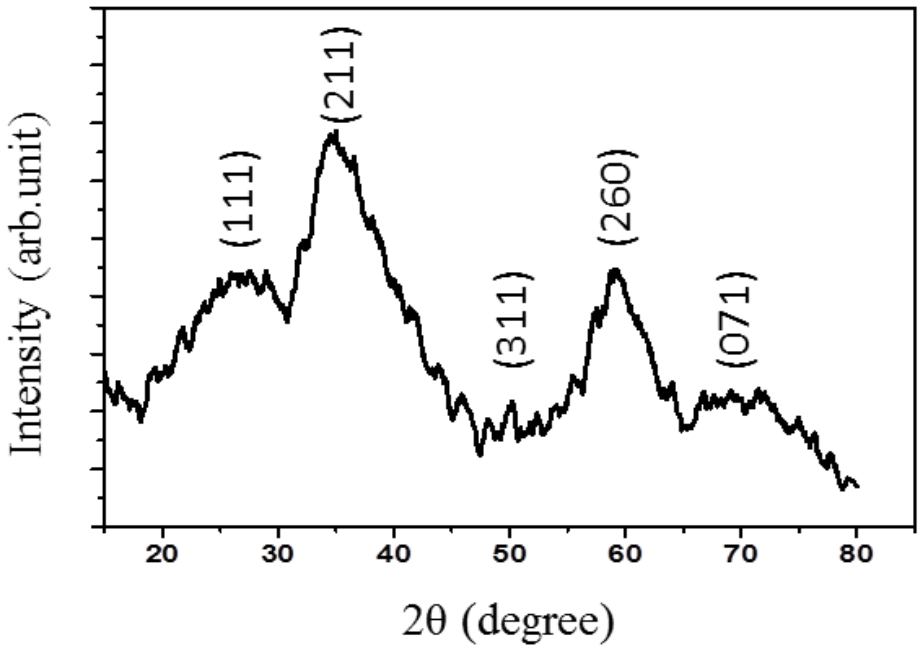


*Figure 4. 2 X-Ray diffraction of the as synthesized $Co_2SiO_4$*

## 4.2 TGA-DTA analysis

The DTA/TGA curves of the thermal degradation of the $Co_2SiO_4$, is shown in Figure 4.3, it indicates that a large weight loss of 17.7% from room temperature to around 230 $^oC$, observed by a broad endothermic peak, that's attributed to the evaporation of adsorbed water. A weight loss of 6.6% from 230 to 254 $^oC$ and an exothermic peak at 254 $^oC$ is observed. This exothermic transition is associated with the burning of the organic residues in the $Co_2SiO_4$ precursor gel. A small weight loss of 0.35% from 255 to 990 $^oC$, observed by exothermic peak at 729$^oC$ which related to the reduction of $Co_3O_4$ to CoO with the corresponding release of O and the formation of $Co_2SiO_4$ [162].

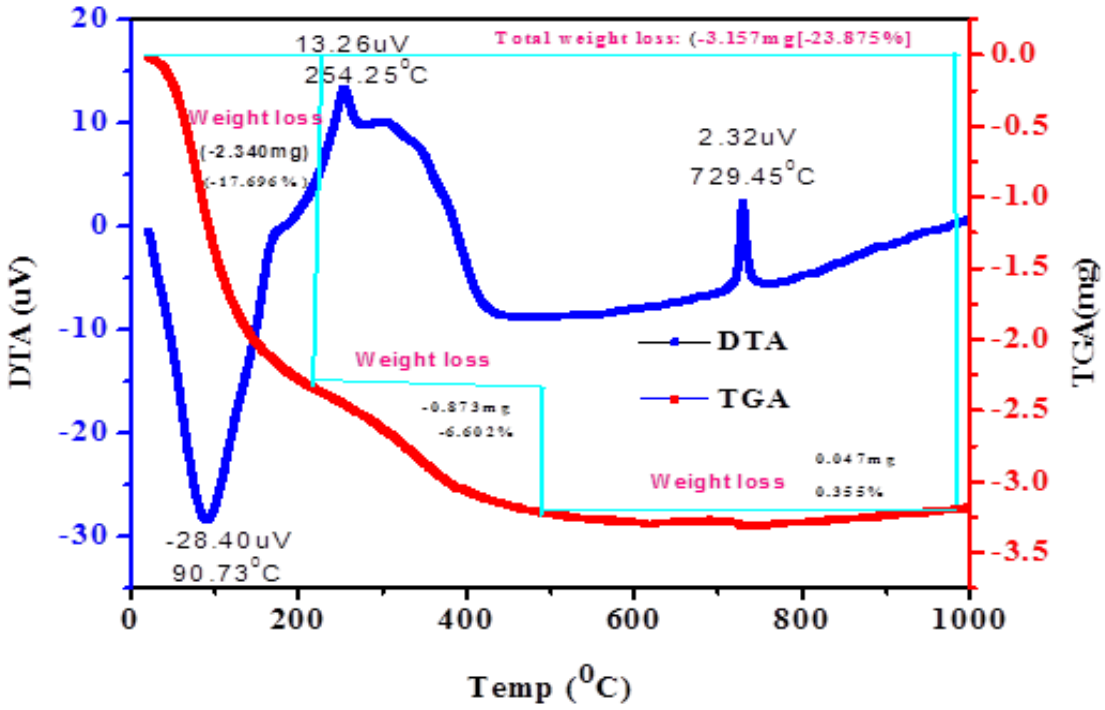


*Figure 4. 3 The DTG-TGA curve for $Co_2SiO_4$ Prepared from sodium silicate as a silicate source*

Based on the information from Figure 4.3, annealing $Co_2SiO_4$ powder at the temperature range between 700-900$^oC$ can make the powder crystal, so that, the diffraction peak can appear. Figure 4.4a, shows that the annealed $Co_2SiO_4$ at 800$^oC$for 3h and the peaks are in good agreement with JCPDS file 00-015-0865. The final product was orthorhombic $Co_2SiO_4$.

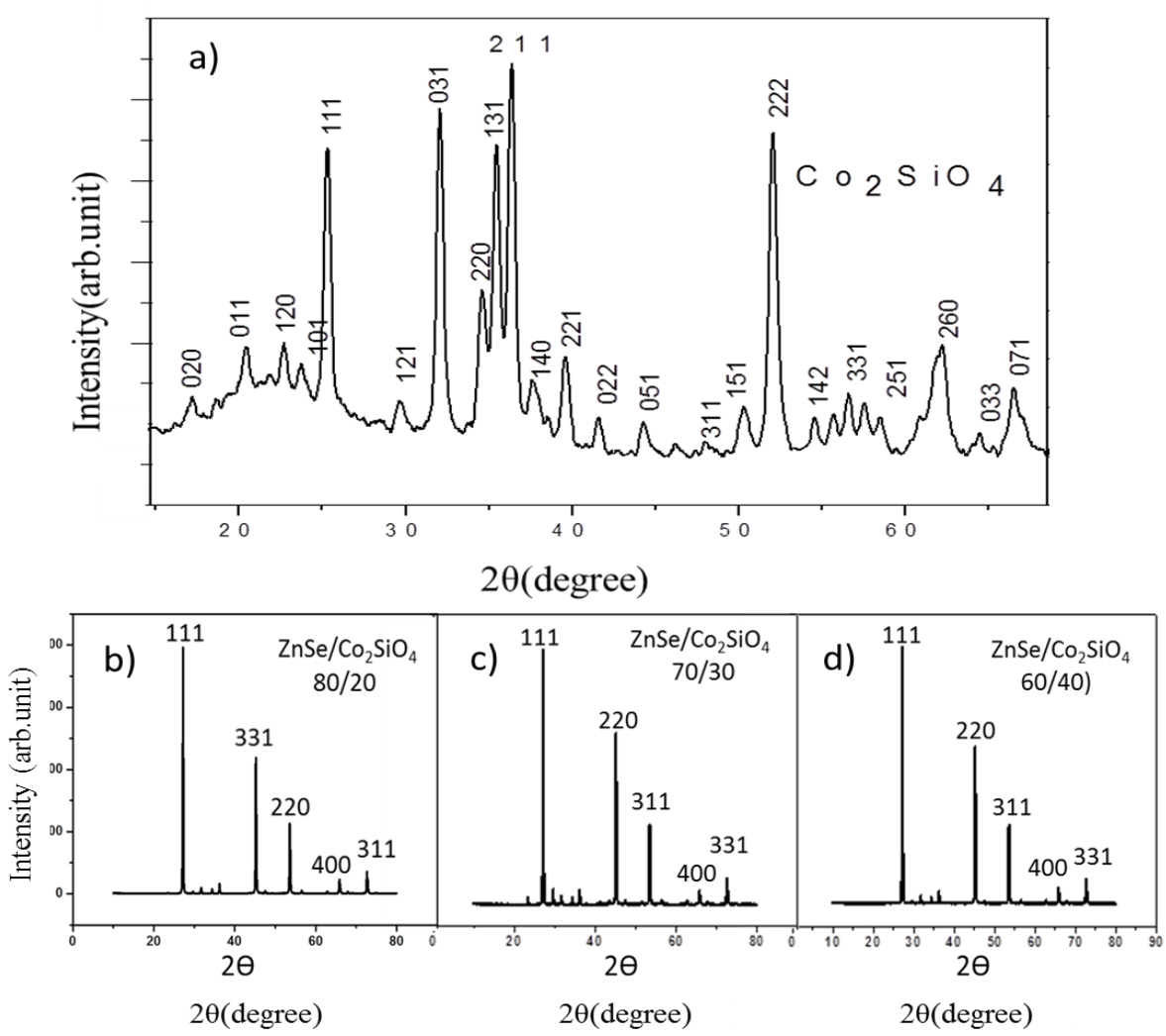


*Figure 4. 4 XRD of a) $Co_2SiO_4$ (annealed at 800$^oC$ for 3h), and b-d) ZnSe/$Co_2SiO_4$ composites.*

The XRD result of hetrostructor ZnSe/$Co_2SiO_4$ is shown in the Figure 4.4 b-d; the result showed that there is no considerable difference from the peak value of pure ZnSe that is due to the amorphous nature of the $Co_2SiO_4$ which can't contribute a peak value in ZnSe/$Co_2SiO_4$ hetrostructure.

The average crystal size was also determined from the full width of the half maximum (FWHM) peak using Scherer formula as follows:

$$D = K\lambda/\beta\text{Cos}\theta \quad \text{..... (1)}$$

Where D = crystallite size K = shape constant i.e. 0.9

$\lambda$ = wavelength of X-ray radiation i.e. 0.15406

$\beta$ = full width at half maxima (FWHM) $\theta$ = diffraction angle

*Table 4. 1 Average crystal size of prepared samples*

| **Samples** | **Average Crystal size ( nm)** |
|---|---|
| ZnSe | 33.94 |
| $Co_2SiO_4$ | 16.05 |
| ZnSe/ $Co_2SiO_4$(80/20) | 34.14 |
| ZnSe/ $Co_2SiO_4$(70/30) | 34.24 |
| ZnSe/ $Co_2SiO_4$(60/40) | 35.38 |

As shown in the table 4.1 the crystal sizes of the composites are nearly equivalent to the crystal size of ZnSe. There is no significant difference in their crystal size. The addition of $Co_2SiO_4$ didn't affect the crystal size of the samples.

## 4.3 Optical property (DRS results)

Studying the optical properties of materials is a convenient and effective way to explain some important properties related to the band structure. The optical properties of ZnSe, $Co_2SiO_4$ and ZnSe/ $Co_2SiO_4$ are analyzed by diffuse reflectance spectroscopy UV-Vis (DRS).The band gap energy (Eg) was calculated by a modified Kubelka-Munk function.[23]

$$F(R) = (1-R)^2/2R = \frac{K}{S} \ldots\ldots\ldots\ldots\ldots\ldots\ldots\ldots\ldots (2)$$

where *K* and *S* are the absorption and scattering coefficients, respectively. The optical absorption spectrum of ZnSe, $Co_2SiO_4$, and ZnSe/ $Co_2SiO_4$ nanostructures represents in Figure. 4.5. Band gap of all the samples was estimated by plotting $(F(R)h\nu)^2$ vs. hν as shown in inset of Figure .4.5 and extrapolating the linear portion near the onset of absorption edge to the energy axis. Therefore, band gap of ZnSe, $Co_2SiO_4$ and ZnSe/ $Co_2SiO_4$ are 2.58eV, 3.2eV, 3.12eV respectivly.

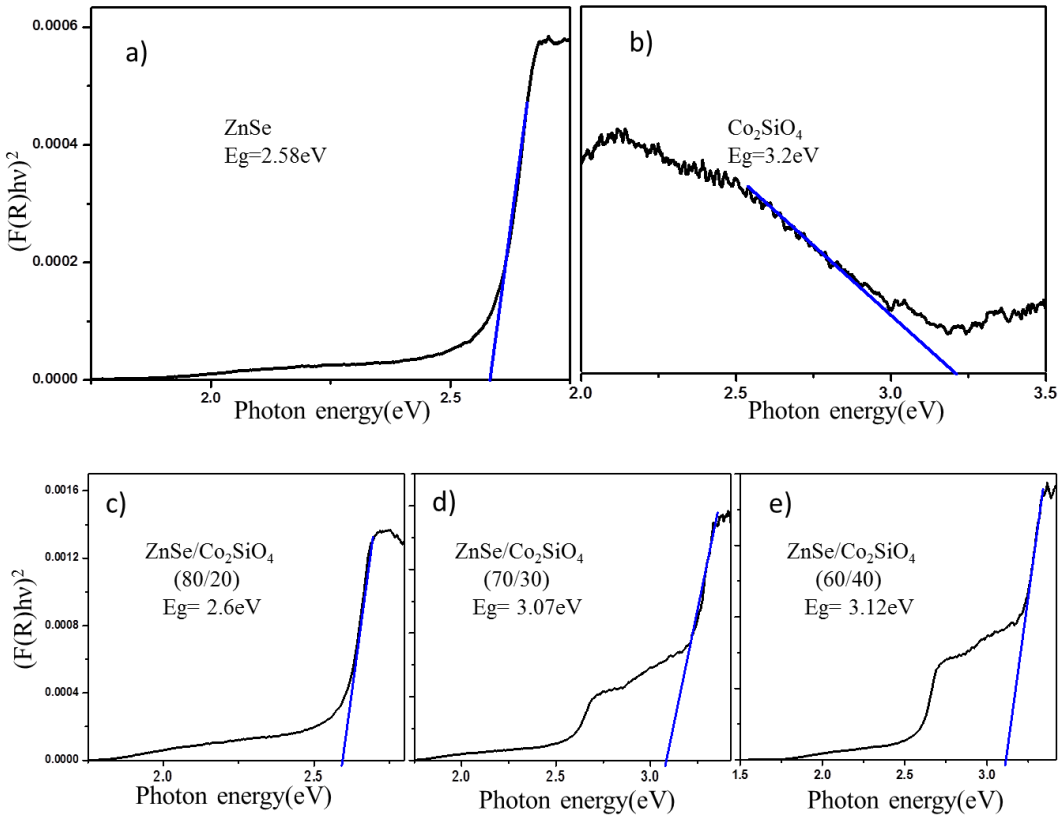


*Figure 4.5 Kubelka plot of synthesized a) ZnSe, b )$Co_2SiO_4$ and c-e) ZnSe/ $Co_2SiO_4$ Composite*

## 4.4 Morphological Analysis

Scanning electron microscope has been used to investigate the structures and morphologies of the synthesized samples. The SEM images of the synthesized samples are shown in Figure 4.6 (a-c). These images indicate that the samples are agglomerated. Fig4.7a shows image of pure ZnSe which composed of small particles with irregularly shaped aggregates. As shown in the fig4.7b the $Co_2SiO_4$ take a random shape of aggregates composed of a large quantity of small flakes. Figure 4.6c shows images of the composite $ZnSe/Co_2SiO_4$. A slight change in the morphologies of the composite can be observed, which result from the addition of $Co_2SiO_4$ to ZnSe.

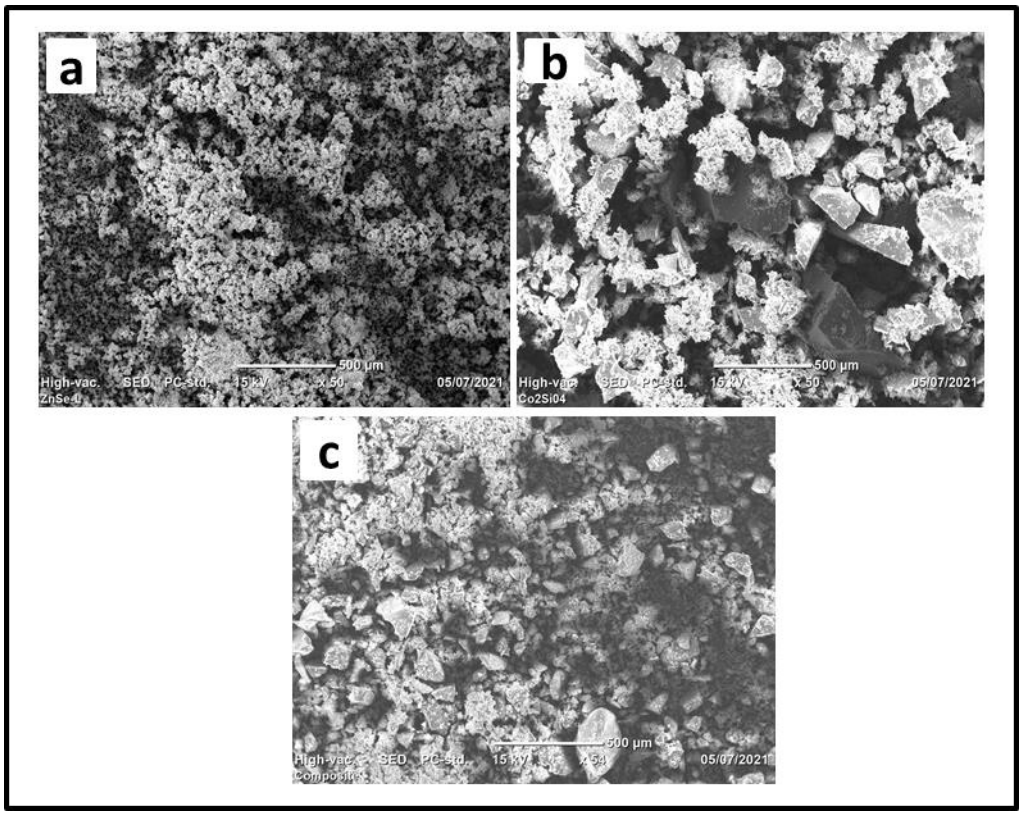


*Figure 4.6 SEM images of a) ZnSe, b) $Co_2SiO_4$, c) $ZnSe/Co_2SiO_4$*

## 4.5 Photoluminescence spectra analysis

The PL emission spectra have been widely used to investigate the efficiency of charge carrier trapping, immigration and transfer, and to understand the fate of electron hole pairs in semiconductor particles. Figure 4.7a shows the PL spectra of ZnSe which exhibited emission peak at 550 nm regions under an excitation wavelength of 250 nm, it has higher intensity peak which indicating that the recombination rate is high. However, the PL intensity of $Co_2SiO_4$ (Figure 4.7b) exhibit a small intensity peak (which indicate the recombination rate in is small) at the same wavelength. Comparing with ZnSe the composite $ZnSe/Co_2SiO_4$(figure 4.7c) shows a small decrease in intensity ($ZnSe > ZnSe/Co_2SiO_4 > Co_2SiO_4$) that is due to the effect result from addition of $Co_2SiO_4$. Therefore, adding $Co_2SiO_4$ on ZnSe result in decreasing the recombination rate of ZnSe and also result for abettor absorption capacity. One of the main contributions to the reduction in the measured luminescence from ZnSe is the suppression of surface recombination of photogenerated electrons and holes in ZnSe at 550nm. In particular, the UV ZnSe emission is reduced when $Co_2SiO_4$ is added. Therefore, it implies that the tendency of surface recombination of electron-hole pairs in $ZnSe/Co_2SiO_4$ composite has been decreased.

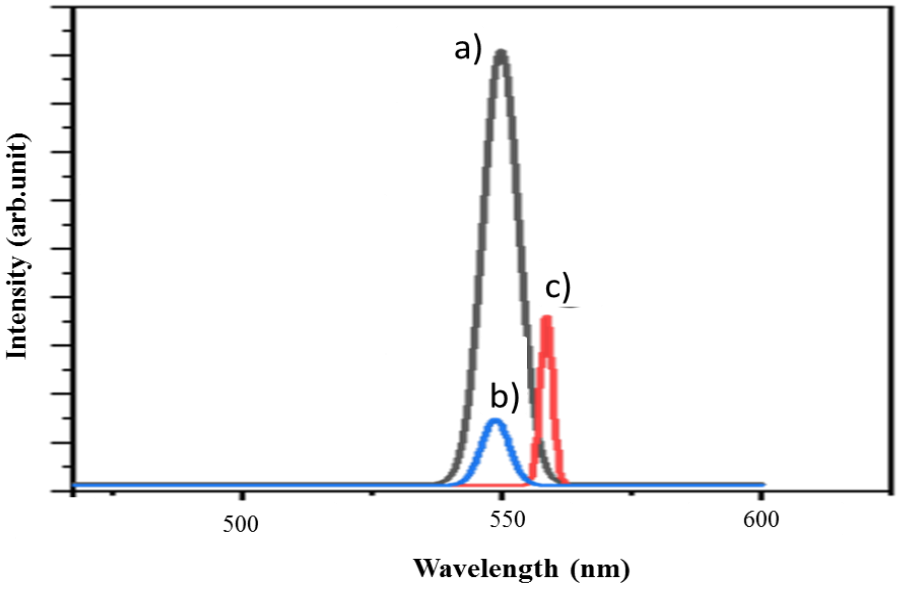


*Figure 4. 7 PL of a) ZnSe, b) $Co_2SiO_4$ and c) $ZnSe/Co_2SiO_4$ (60/40)*

## 4.6 FTIR results

Fourier transform infrared spectroscopy (FTIR) is an important analytical method for determining functional groups and confirming the presence of chemical bonding in semiconductor compounds. Therefore, the FT-IR spectra of the synthesized ZnSe, $Co_2SiO_4$ and $ZnSe/Co_2SiO_4$ are taken in the range of 4000-400 $cm^{-1}$ at room temperature, see Figure 4.8.

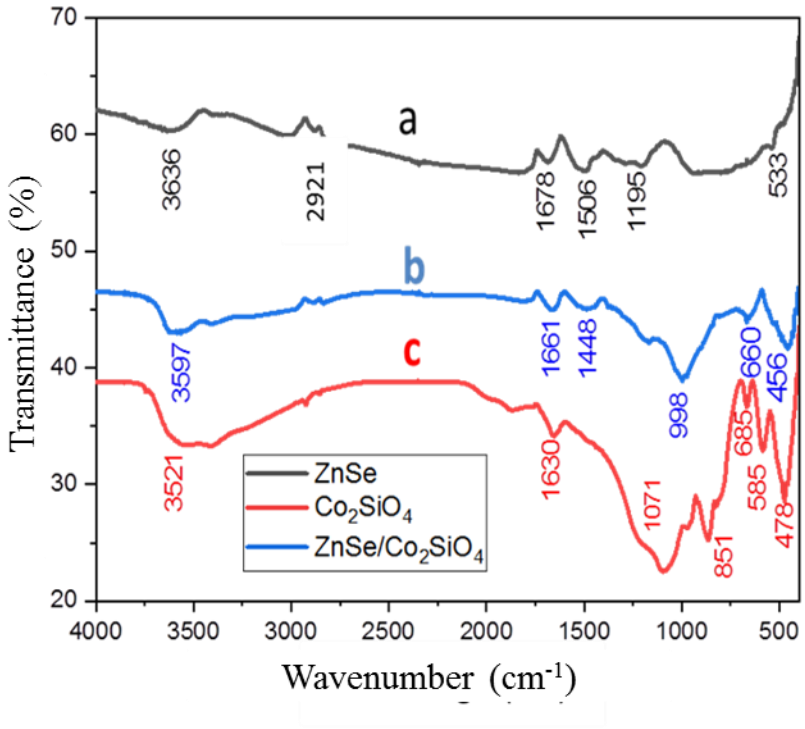


*Figure 4. 8 FTIR of a) ZnSe, b) $ZnSe/Co_2SiO_4$ and c) $Co_2SiO_4$*

In Figure 4.8 the FTIR spectra of ZnSe, $Co_2SiO_4$, and $ZnSe/Co_2SiO_4$ composites are compared. The FTIR peaks of the $ZnSe/Co_2SiO_4$ composites exist in both ZnSe and $Co_2SiO_4$, proving that $ZnSe/Co_2SiO_4$ composites are obtained.

In Figure 4.8 curve 'a' shows the FTIR spectra of ZnSe, under this curve, the characteristic major peak appearing at 533 $cm^{-1}$ belongs to Zn-Se vibrations. The broad peak at 3636 $cm^{-1}$ and the weak peak at 1678 $cm^{-1}$ are assigned to O-H characteristic vibrations resulting from all small quantity of $H_2O$ in the sample[158]. The band at 2,921 $cm^{-1}$ was ascribed to the asymmetric stretching of C–H[98,159].

Furthermore, the absorption peak at 1506 $cm^{-1}$ corresponds to vibration due to C-H bending in the methylene group, while the peak at 1195$cm^{-1}$ is associated with C-N stretching vibration[160]. whereas curve 'c' in Figure 4.8 shows the FTIR of $Co_2SiO_4$, the Peak at 1630 $cm^{-1}$ is related to carboxyl stretching mode and the absorption band at 1071$cm^{-1}$ is assigned to the Si-O. The absorption bands at 685,585 and 478$cm^{-1}$ are assigned to the Co-O (metal-oxygen) stretching mode[98]. The peaks at about 851 $cm^{-1}$ can be assigned to the $SiO_4$ tetrahedron vibrations[97]. The cure 'b' in figure 4.9 shows the absorption peak at 3597 and 1661$cm^{-1}$ which indicate the stretching and bending vibration of O-H groups of adsorbed water molecules in the sample. While the peak at 998, 660 and 456$cm^{-1}$ are associated with Si-O, Co-O stretching and Zn-Se vibrations, respectively.

## 4.7 Photocatalytic Dye Degradation activity

The degradation potential of ZnSe, $Co_2SiO_4$, and ZnSe/$Co_2SiO_4$ hetrostructure are investigated under visible light, methyl blue (MB) was selected as the target pollutant. 50 mg of each powdered sample were transferred to 100 ml of stock MB solution. The concentration of MB is monitored as a function of time, in every 15min. Figure 4.9 demonstrates the visible absorption spectrum of degraded MB solution. As shown in Figure 4.9, the maximum peak at 660 nm abruptly decreased the intensity in 30 min dark reaction due to the dye adsorption ability of the catalyst. Moreover, when the time passes by the intensity gradually decreased under visible light irradiation. The result shows, with increasing the reaction time, the absorption peaks of three samples gradually decreased, and methyl blue degraded with time. Compared with ZnSe (Figure 4.9a) and $Co_2SiO_4$ (Figure 4.9b), the heterostructure of ZnSe/$Co_2SiO_4$ exhibited stronger degradation potential, It is also indicated that the adsorption of MB dye under dark was maximum and makes the pollutant concentration lower in the solution. Moreover, the degradation of MB dye with ZnSe/$Co_2SiO_4$ also further enhanced, which was caused by the effective separation of electron–holes pair of composite (Figure 4.9c, d, e).

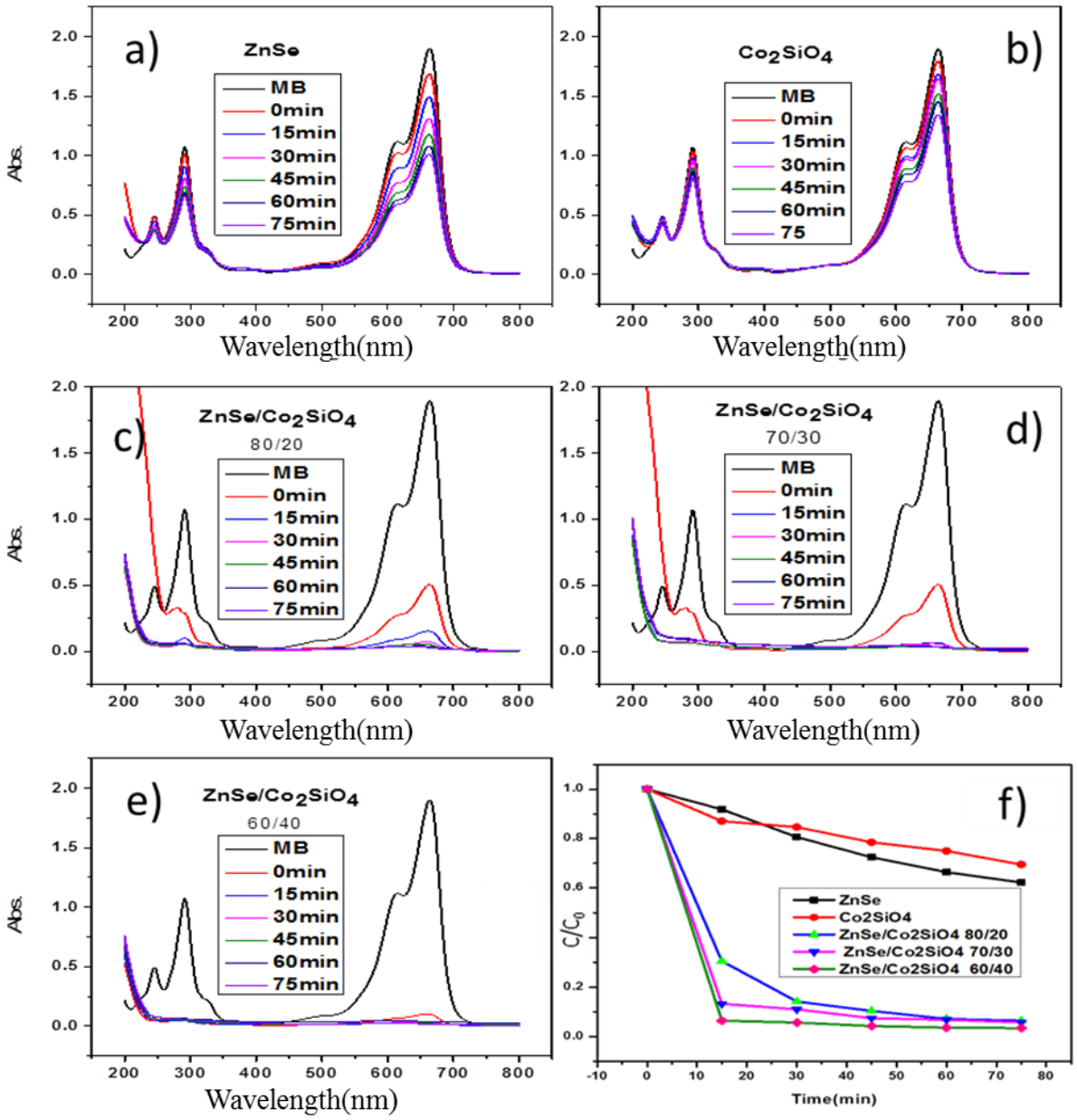


*Figure 4. 9 The visible light absorption spectra of methylene blue (MB) observed at regular time intervals, with the (a) ZnSe, (b) $Co_2SiO_4$, (c) $ZnSe/Co_2SiO_4$ (80/20), d) $ZnSe/Co_2SiO_4$(70/30, e) $ZnSe/Co_2SiO_4$(60/40)samples and f) $C/C_0$ photocatalytic degradation rates of ) ZnSe, $Co_2SiO_4$ and ZnSe/ $Co_2SiO_4$ composites.*

The photocatalytic degradation rate of Methyl Blue in ZnSe, $Co_2SiO_4$ and ZnSe/ $Co_2SiO_4$ samples were shown in Figure. 4.9f, ($C/C_0$ where $C_0$ is the initial absorbance and C is the absorbance at time t). As can be seen, the degradation rat of ZnSe/$Co_2SiO_4$ (60/40) is higher than from all. To demonstrate this point, the photocatalytic rate constant for the MB degradation (*k*) was also determined by Langmuir–Hinshelwood pseudo-first order kinetic equation.[161]

$$\ln\left(\frac{C0}{Ct}\right) = Kt \ldots\ldots\ldots\ldots\ldots\ldots\ldots\ldots\ldots\ldots\ldots\ldots\ldots\ldots (4)$$

Where *k* is the first-order rate constant.

Figure 4.10B presents the results of this plot for all samples. As can be seen, the constant rate of the ZnSe, $Co_2SiO_4$ and ZnSe/$Co_2SiO_4$(60/40) is 0.00656, 0.0445 and 0.03607 respectively. Therefore, The degradation constant rate of MB over ZnSe/$Co_2SiO_4$(60/40) is 5.5 and 8 times higher than that of pure ZnSe and $Co_2SiO_4$ respectively, indicating that the degradation rate of MB in ZnSe/$Co_2SiO_4$(60/40) is very fast.

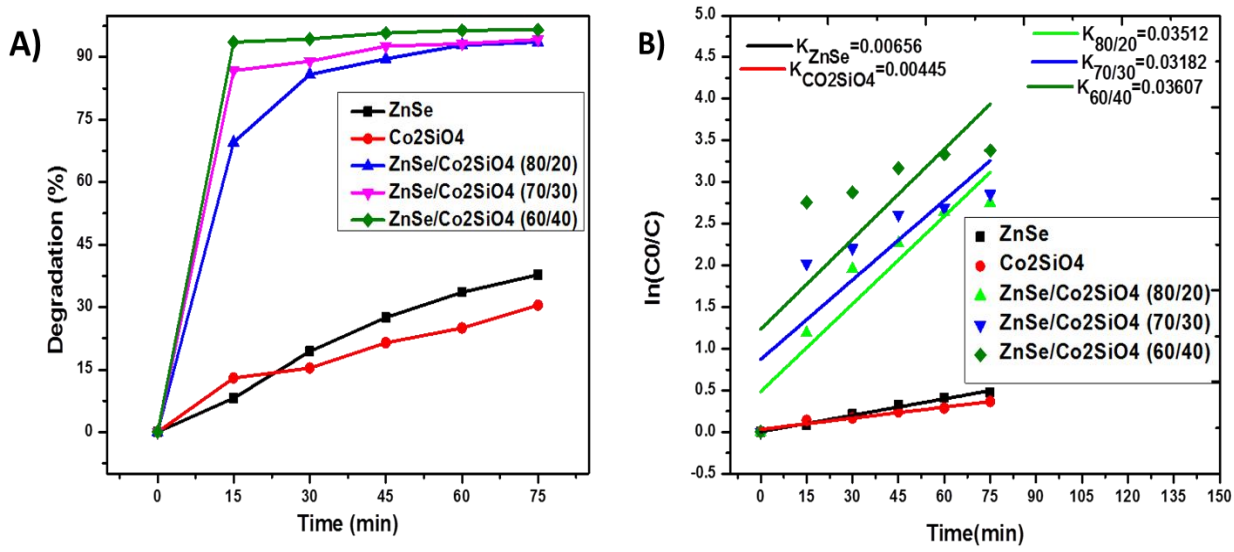


*Figure 4. 10 A) % degradation of methylene blue (MB) observed at regular time intervals, with the ZnSe, $Co_2SiO_4$ and ZnSe/ $Co_2SiO_{4\ (60/40)}$ samples B) ln($C_0$/C) versus irradiation time for different photocatalysts*

According to the Beer–Lambert law, the change in the concentration of organic pollutant MB in aqueous solution is directly proportional to the change in intensity of the absorption peak, therefore the percentage degradation efficiency of MB is measured by applying the following expression[64][140].

$$\%Degradation = \frac{C0-Ct}{C0} * 100 \quad \text{..... (5)}$$

Where $C_0$ is the initial concentrarion of MB, $C_t$ is the concentration of MB at a given time t. As shown in the Figure 4.10A, the degradation potential of ZnSe and $Co_2SiO_4$ after 75min irradiation treatment was about 37.7% and 30.5% respectively, however the degradation potential of ZnSe/ $Co_2SiO_4$ (80/20), ZnSe/$Co_2SiO_4$ (70/30), ZnSe/$Co_2SiO_4$(60/40) hetrostructures after 75min irradiation time are 93.6%,94.3%,96.6% respectively.

*Table 4. 2 degradation efficiency of samples with respective irradiation time*

| **Degradation of MB in Percentage (%)** | | | | | | |
|---|---|---|---|---|---|---|
| | **0min** | **15min** | **30min** | **45min** | **60min** | **75min** |
| **ZnSe** | 0% | 8.1 % | 19.3% | 27.5% | 33.5% | 37.7% |
| **$Co_2SiO_4$** | 0% | 12.9% | 15.3% | 21.4% | 24.9% | 30.5% |
| **ZnSe/$Co_2SiO_4$ (80/20)** | 0% | 69.5% | 85.9% | 89.6% | 92.9% | 93.6% |
| **ZnSe/$Co_2SiO_4$ (70/30)** | 0% | 86.7% | 89.0% | 92.6% | 93.2% | 94.3% |
| **ZnSe/$Co_2SiO_4$ (60/40)** | 0% | 93.6% | 94.4% | 95.8% | 96.4% | 96.6% |

Table 4.2 shows summery of the degradation efficiency of samples, Comparing all, ZnSe/$Co_2SiO_4$ (60/40) exhibit the highest degradation performance and this indicate the molar ratio of ZnSe to $Co_2SiO_4$ play a great role in degradation of MB. Furthermore, the result implies that formation of ZnSe/$Co_2SiO_4$ composite leds to have better degradation efficiency than the pure ZnSe and $Co_2SiO_4$.

### 4.7.1 Images of Degraded methylene blue

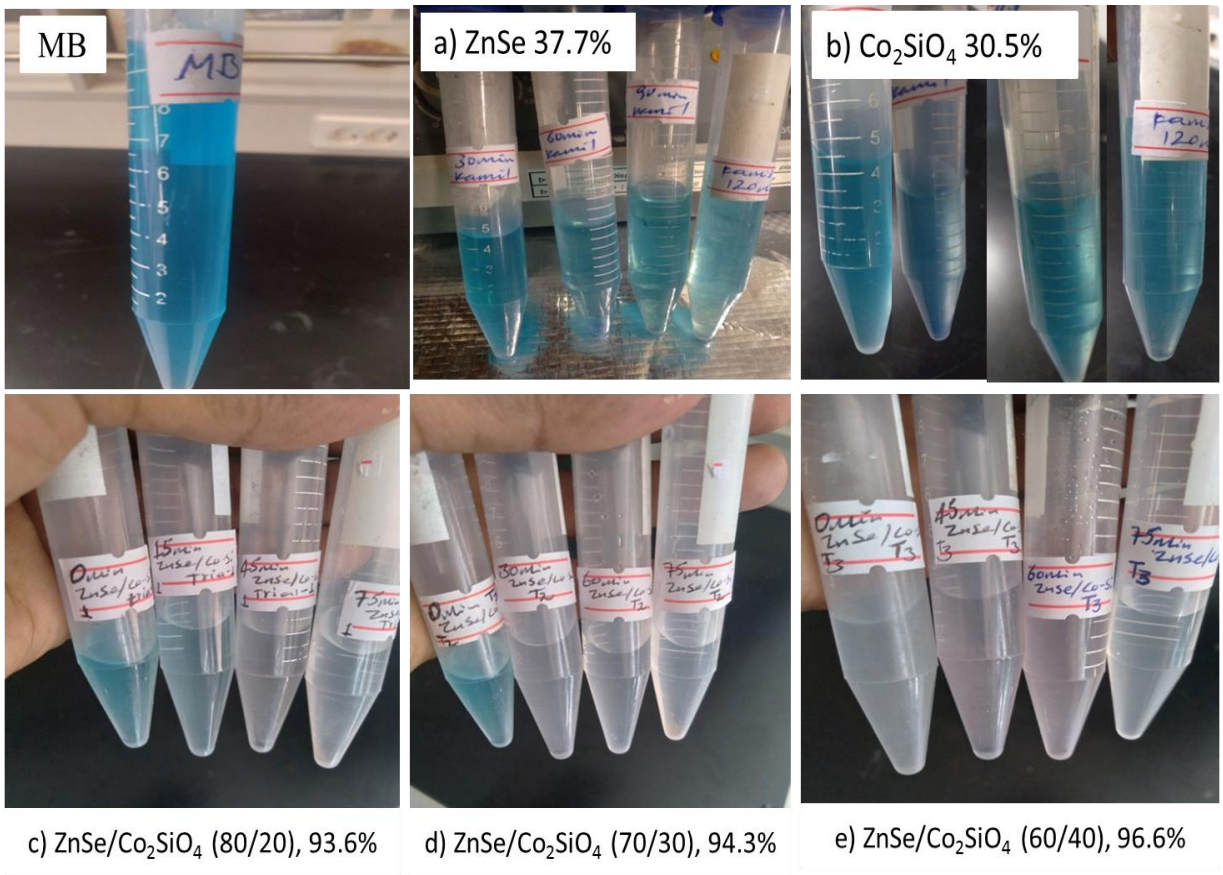


*Figure 4.11 Images of degraded methylene blue*

*Table 4. 3 The pseudo-first order rate constant (k) and Average value of $C/C_0$ of samples*

| | **$C/C_0$** | **$K(min^{-1})$** | **Degradation% in 75min** |
|---|---|---|---|
| **ZnSe** | 0.79 | 0.0066 | 37.7% |
| **$Co_2SiO_4$** | 0.82 | 0.0044 | 30.5% |
| **$ZnSe/Co_2SiO_4$ (80/20)** | 0.28 | 0.0351 | 93.6% |
| **$ZnSe/Co_2SiO_4$ (70/30)** | 0.24 | 0.0318 | 94.3% |
| **$ZnSe/Co_2SiO_4$ (60/40)** | 0.20 | 0.0360 | 96.6% |

In general, the highest degradation rate of $ZnSe/Co_2SiO_4$ sample could be explained by absorption potential and effective charge carrier separation that could be improved due to the coupling and co-catalyst effect between ZnSe and $Co_2SiO_4$. So that the improved electron transport ability could greatly inhibit the recombination probability of charge carriers in $ZnSe/Co_2SiO_4$, which can significantly enhance their photocatalytic activity. On the other hand, the slightly exposed active surface of ZnSe was sensitive to the process of promoting surface carrier transfer.

The first order kinetics equation $\ln(C_0/C) = kt$ is used to calculate the rat constant of MB on the photocatalysis, Figure 4.10b shows $\ln(C_0/C)$ versus irradiation time for different photocatalysts. Also, the above table4.3 shows The pseudo-first-order rate constant (k) and average value of $C/C_0$ of samples.

## 4.8 Recyclability Test

According to reports, selenide-based photocatalysts may have the problem of photocorrosion and oxidation during repeated photocatalytic processes that generate selenide ions, [34] and the photocatalytic activity process must be stable and reusable in industrial applications. Cyclic photocatalytic activity is carried out under visible light irradiation to decompose MB dye. After four photocatalytic cycles, the photocatalytic material was reused by centrifuging the MB and washing the nanostructures. The result of the reuse test is shown in Figure 4.12. For the $ZnSe/Co_2SiO_4$(60/40) composite, slight difference were observed after 75 minutes of each irradiation.

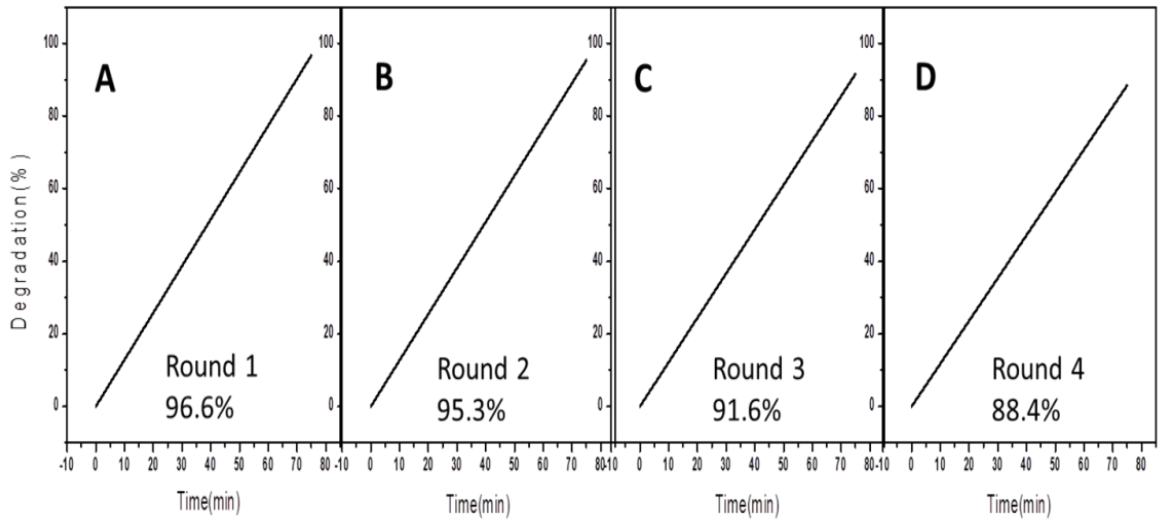


*Figure 4.12 Recycling experiments for the degradation of MB using $ZnSe/Co_2SiO_4$(60/40) as photocatalys*

## 4.9 Possible Photocatalytic Mechanism

The possible catalytic mechanism is proposed and illustrated in Figure 4.13. ZnSe can absorb the photon energy under light irradiation, and the electrons in the valence band (VB) are excited to the conduction band (CB) to generate the electron-hole pairs. Subsequently, the electrons and holes migrate to the surface of the photocatalysts to participate in redox reactions. Photo-excitation of the electron from ZnSe to the $Co_2SiO_4$ assists charge separation by generating more •OH radicals for the degradation of dye molecules. Holes from the valence band breaks the H2O and leads to the formation of •OH radicals, hence in-turn degrade the dye molecules. The CB e- reacts with $O_2$ molecule to form a super oxide ion ($•O^{2-}$), which can also react with further dye molecules. Thus overall the active species generated enhances the photocatalytic process. The photogenerated electron of ZnSe are captured and transferred by $Co_2SiO_4$, thereby reducing the recombination rate of photoelectron-hole pairs. Overall the photocatalytic efficacy of the prepared composite is due to the cumulative contribution from ZnSe and Co2SiO4. The adsorption ability of the composites is enhanced by the presence of the $Co_2SiO_4$. The synergistic effect between $Co_2SiO_4$,and ZnSe in the ZnSe/$Co_2SiO_4$ composite allows $Co_2SiO_4$ to capture or trap the photo-induced electrons from the conduction band of the ZnSe, and consequently restrict recombination of electron–hole pair. Therefore, ZnSe/$Co_2SiO_4$ is expected to show higher photocatalytic activity.

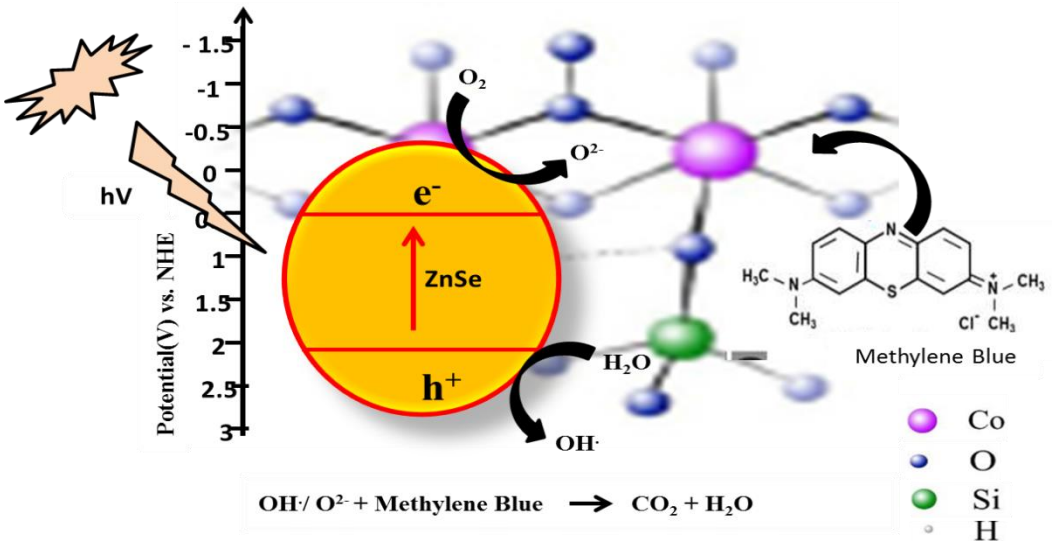


*Figure 4.13 Proposed photocatalytic dye degradation mechanism*

# 5 Conclusion

We have successfully synthesized ZnSe, $Co_2SiO_4$ and ZnSe/$Co_2SiO_4$ photocatlysts using solvothermal and sol-gel method respectively. The X-ray diffraction, UV–Vis diffuse reflectance spectroscopy (DRS), Photoluminescence (PL), Fourier transform Infrared (FT-IR) and SEM were used for characterization of the synthesized samples. The effects of $Co_2SiO_4$ on the photocatalytic performance of ZnSe under a visible-light source irradiation were investigated. The synthesized ZnSe/$Co_2SiO_4$ composites exhibited excellent photocatalytic performance on the degradation of MB, which was superior over those of pure ZnSe and $Co_2SiO_4$ under visible light (96.6%, 37.7% and 30.5% respectively). Therefore, hetrostructure of the ZnSe and $Co_2SiO_4$ was important for enhanced photocatalytic performance of the ZnSe/$Co_2SiO_4$ composites due to decreasing the recombination process of electron-hole pairs and improve the absorption capacity. However, the molar ratios of ZnSe to $Co_2SiO_4$ affect the photocatalytic activity of the composite, ZnSe/$Co_2SiO_4$. So that superior degradation potential of the ZnSe/$Co_2SiO_4$ heterostructures was observed with the molar ratios of 60%/40%, ZnSe/$Co_2SiO_4$ (60/40) (about 96.6%). The cocatlyst effects of $Co_2SiO_4$ also play a great role in photocatlytic performance of ZnSe/$Co_2SiO_4$. Moreover, ZnSe/$Co_2SiO_4$ exhibited good stability in the photocatalytic process under visible light irradiation. Based on the results of this study, addition of $Co_2SiO_4$ in ZnSe could be the best approach to improve the photocatlytic performance of ZnSe. Also, ZnSe/$Co_2SiO_4$ composite is expected to be effective and useful visible light photocatalyst for practical applications.

# Reference

[1] R. Molinari, C. Grande, E. Drioli, L. Palmisano, and M. Schiavello, "Photocatalytic membrane reactors for degradation of organic pollutants in water," vol. 67, pp. 273–279, 2001.

[2] A. P. Shah, S. Jain, V. J. Mokale, and N. G. Shimpi, "High performance visible light photocatalysis of electrospun PAN/ZnO hybrid nanofibers," *J. Ind. Eng. Chem.*, vol. 77, pp. 154–163, 2019, doi: 10.1016/j.jiec.2019.04.030.

[3] D. Liu, X. Li, Z. Shi, B. Zhu, X. Chen, and J. Yang, "Synthesis of porous ZnS / ZnSe nanosheets for enhanced visible light photocatalytic activity," *J. Mater. Sci. Mater. Electron.*, vol. 0, no. 0, p. 0, 2018, doi: 10.1007/s10854-018-9258-y.

[4] L. Zang, *Energy Efficiency and Renewable Energy Through Nanotechnology*, vol. 33. 2011.

[5] K. Elatmani, N. Ben oujji, G. Plantara, V. Goetz, and I. A. ichou, "3D Photocatalytic media for decontamination of water from pesticides," *Mater. Res. Bull.*, vol. 101, no. 2010, pp. 6–11, 2018, doi: 10.1016/j.materresbull.2017.12.042.

[6] N. Vela *et al.*, "Photocatalytic oxidation of six pesticides listed as endocrine disruptor chemicals from wastewater using two different TiO2 samples at pilot plant scale under sunlight irradiation," *J. Photochem. Photobiol. A Chem.*, vol. 353, pp. 271–278, 2018, doi: 10.1016/j.jphotochem.2017.11.040.

[7] A. Sraw, T. Kaur, Y. Pandey, A. Sobti, R. K. Wanchoo, and A. P. Toor, "Fixed bed recirculation type photocatalytic reactor with TiO2 immobilized clay beads for the degradation of pesticide polluted water," *J. Environ. Chem. Eng.*, vol. 6, no. 6, pp. 7035–7043, 2018, doi: 10.1016/j.jece.2018.10.062.

[8] S. G. Babu *et al.*, "Synergistic effect of sono-photocatalytic process for the degradation of organic pollutants using CuO-TiO2/rGO," *Ultrason. Sonochem.*, vol. 50, pp. 218–223, 2019, doi: 10.1016/j.ultsonch.2018.09.021.

[9] S. Kumar, C. Terashima, and A. Fujishima, *Photocatalytic Degradation of Organic Pollutants in Water Using Graphene Oxide Composite*. Springer International Publishing, 2019.

[10] L. Rojas-blanco, L. L. Díaz-flores, G. E. Sepúlveda-palacios, and F. Paraguay-delgado, "Eu-modi fi ed ZnO nanoparticles for applications in photocatalysis," vol. 349, no. October 2017, pp. 191–197, 2020, doi: 10.1016/j.cattod.2018.04.060.

[11] Q. Zhang *et al.*, "Effects of calcination temperature on crystal structure and photocatalytic activity of CaIn2O4/ In2O3 composites," *Ceram. Int.*, vol. 45, no. 17, pp. 21851–21857, 2019, doi: 10.1016/j.ceramint.2019.07.194.

[12] Y. Wang, Q. Wang, X. Zhan, F. Wang, M. Safdar, and J. He, "Visible light driven type II heterostructures and their enhanced photocatalysis properties: A review," *Nanoscale*,

vol. 5, no. 18, pp. 8326–8339, 2013, doi: 10.1039/c3nr01577g.

[13] T. Bora, P. Sathe, K. Laxman, S. Dobretsov, and J. Dutta, "Defect engineered visible light active ZnO nanorods for photocatalytic treatment of water," *Catal. Today*, vol. 284, pp. 11–18, 2017, doi: 10.1016/j.cattod.2016.09.014.

[14] N. Raza, W. Raza, H. Gul, and K. H. Kim, "ZnO–ZnTe hierarchical superstructures as solar-light-activated photocatalysts for azo dye removal," *Environ. Res.*, vol. 194, p. 110499, 2021, doi: 10.1016/j.envres.2020.110499.

[15] A. Shirmardi, M. A. M. Teridi, H. R. Azimi, W. J. Basirun, F. Jamali-Sheini, and R. Yousefi, "Enhanced photocatalytic performance of ZnSe/PANI nanocomposites for degradation of organic and inorganic pollutants," *Appl. Surf. Sci.*, vol. 462, pp. 730–738, 2018, doi: 10.1016/j.apsusc.2018.06.252.

[16] T. D. Nguyen-Phan *et al.*, "Fabrication of TiO2 nanostructured films by spray deposition with high photocatalytic activity of methylene blue," *Mater. Lett.*, vol. 64, no. 12, pp. 1387–1390, 2010, doi: 10.1016/j.matlet.2010.03.033.

[17] J. Marto, P. S. Marcos, T. Trindade, and J. A. Labrincha, "Photocatalytic decolouration of Orange II by ZnO active layers screen-printed on ceramic tiles," *J. Hazard. Mater.*, vol. 163, no. 1, pp. 36–42, 2009, doi: 10.1016/j.jhazmat.2008.06.056.

[18] L. Zhao, C. Sun, G. Tian, and Q. Pang, "Multiple-shell ZnSe core-shell spheres and their improved photocatalytic activity," *J. Colloid Interface Sci.*, vol. 502, pp. 1–7, 2017, doi: 10.1016/j.jcis.2017.04.056.

[19] E. Evgenidou, I. Konstantinou, K. Fytianos, I. Poulios, and T. Albanis, "Photocatalytic oxidation of methyl parathion over TiO2 and ZnO suspensions," *Catal. Today*, vol. 124, no. 3–4, pp. 156–162, 2007, doi: 10.1016/j.cattod.2007.03.033.

[20] L. Y. Yang, S. Y. Dong, J. H. Sun, J. L. Feng, Q. H. Wu, and S. P. Sun, "Microwave-assisted preparation, characterization and photocatalytic properties of a dumbbell-shaped ZnO photocatalyst," *J. Hazard. Mater.*, vol. 179, no. 1–3, pp. 438–443, 2010, doi: 10.1016/j.jhazmat.2010.03.023.

[21] L. Liu, Y. Zhang, and H. Huang, "Junction Engineering for Photocatalytic and Photoelectrocatalytic CO2 Reduction," *Sol. RRL*, vol. 5, no. 2, 2021, doi: 10.1002/solr.202000430.

[22] J. Low, J. Yu, M. Jaroniec, S. Wageh, and A. A. Al-Ghamdi, "Heterojunction Photocatalysts," *Adv. Mater.*, vol. 29, no. 20, pp. 1–20, 2017, doi: 10.1002/adma.201601694.

[23] N. G. Kostova, M. Achimovicova, and M. Fabian, "Photocatalytic behavior of ZnSe-TiO2 composite for degradation of methyl orange dye under visible light irradiation," *Bulg. Chem. Commun.*, vol. 51, no. 3, pp. 439–444, 2019, doi: 10.34049/bcc.51.3.5142.

[24] H. Xu *et al.*, "Synthesis, characterization and photocatalytic property of AgBr/BiPO 4 heterojunction photocatalyst," *Dalt. Trans.*, vol. 41, no. 12, pp. 3387–3394, 2012, doi:

10.1039/c2dt11969b.

[25] M. F. Ehsan *et al.*, "One-pot facile synthesis of the ZnO/ZnSe heterostructures for efficient photocatalytic degradation of azo dye," *Appl. Surf. Sci.*, vol. 459, no. July, pp. 194–200, 2018, doi: 10.1016/j.apsusc.2018.07.162.

[26] S. Wang *et al.*, *A plate-on-plate sandwiched Z-scheme heterojunction photocatalyst: BiOBr-Bi 2 MoO 6 with enhanced photocatalytic performance*, vol. 391. Elsevier B.V., 2017.

[27] T. T. T. Dang, S. T. T. Le, D. Channei, W. Khanitchaidecha, and A. Nakaruk, "Photodegradation mechanisms of phenol in the photocatalytic process," *Res. Chem. Intermed.*, vol. 42, no. 6, pp. 5961–5974, 2016, doi: 10.1007/s11164-015-2417-3.

[28] Y. Gu, C. Sun, C. Zhang, X. Luo, C. Xue, and L. Zhao, "Inverted ZnSe/CdSe core-shell nanobelts with type-I behavior: Preparation, photoelectrochemical and photocatalytic performances," *CrystEngComm*, vol. 21, no. 36, pp. 5482–5491, 2019, doi: 10.1039/c9ce00958b.

[29] S. H. Hsieh, W. J. Chen, and T. H. Yeh, "Effect of various amounts of graphene oxide on the degradation characteristics of the ZnSe/graphene nanocomposites," *Appl. Surf. Sci.*, vol. 358, pp. 63–69, 2015, doi: 10.1016/j.apsusc.2015.08.220.

[30] M. F. Ehsan *et al.*, "One-pot facile synthesis of the ZnO/ZnSe heterostructures for efficient photocatalytic degradation of azo dye," *Appl. Surf. Sci.*, vol. 459, pp. 194–200, 2018, doi: 10.1016/j.apsusc.2018.07.162.

[31] M. F. Ehsan *et al.*, "ZnTe/ZnSe heterostructures: In-situ synthesis, characterization and photocatalytic activity for Congo Red degradation," *SN Appl. Sci.*, vol. 1, no. 3, pp. 1–9, 2019, doi: 10.1007/s42452-019-0220-2.

[32] M. Zulfiqar, M. Fakhrul, R. Samsudin, and S. Sufian, "Journal of Photochemistry & Photobiology A : Chemistry Modelling and optimization of photocatalytic degradation of phenol via TiO2 nanoparticles : An insight into response surface methodology and artificial neural network," *J. Photochem. Photobiol. A Chem.*, vol. 384, no. August, p. 112039, 2019, doi: 10.1016/j.jphotochem.2019.112039.

[33] M. F. R. Samsudin, P. J. Jayabalan, W. J. Ong, Y. H. Ng, and S. Sufian, "Photocatalytic degradation of real industrial poultry wastewater via platinum decorated BiVO 4 /g-C 3 N 4 photocatalyst under solar light irradiation," *J. Photochem. Photobiol. A Chem.*, vol. 378, no. January, pp. 46–56, 2019, doi: 10.1016/j.jphotochem.2019.04.013.

[34] N. Roostaei and F. H. Tezel, "Removal of phenol from aqueous solutions by adsorption," *J. Environ. Manage.*, vol. 70, no. 2, pp. 157–164, 2004, doi: 10.1016/j.jenvman.2003.11.004.

[35] H. Lin, N. Oturan, J. Wu, V. K. Sharma, H. Zhang, and M. A. Oturan, "Removal of artificial sweetener aspartame from aqueous media by electrochemical advanced oxidation processes," *Chemosphere*, vol. 167, pp. 220–227, 2017, doi: 10.1016/j.chemosphere.2016.09.143.

[36] B. P. Chaplin, "Critical review of electrochemical advanced oxidation processes for water treatment applications," *Environ. Sci. Process. Impacts*, vol. 16, no. 6, pp. 1182–1203, 2014, doi: 10.1039/c3em00679d.

[37] W. Shi and N. Chopra, "Nanoscale heterostructures for photoelectrochemical water splitting and photodegradation of pollutants," *Nanomater. Energy*, vol. 2, no. 3, pp. 158–178, 2013, doi: 10.1680/nme.13.00009.

[38] H. M. Chen, C. K. Chen, R. S. Liu, L. Zhang, J. Zhang, and D. P. Wilkinson, "Nano-architecture and material designs for water splitting photoelectrodes," *Chem. Soc. Rev.*, vol. 41, no. 17, pp. 5654–5671, 2012, doi: 10.1039/c2cs35019j.

[39] A. B. Djurišić, Y. He, and A. M. C. Ng, "Visible-light photocatalysts: Prospects and challenges," *APL Mater.*, vol. 8, no. 3, 2020, doi: 10.1063/1.5140497.

[40] Z. Ye, L. Kong, F. Chen, Z. Chen, Y. Lin, and C. Liu, "A comparative study of photocatalytic activity of ZnS photocatalyst for degradation of various dyes," *Optik (Stuttg).*, vol. 164, pp. 345–354, 2018, doi: 10.1016/j.ijleo.2018.03.030.

[41] R. Peymanfar and H. Ramezanalizadeh, "Optik Sol-gel assisted synthesis of CuCr 2 O 4 nanoparticles : An e ffi cient visible-light driven photocatalyst for the degradation of water pollutions," *Opt. - Int. J. Light Electron Opt.*, vol. 169, no. March, pp. 424–431, 2018, doi: 10.1016/j.ijleo.2018.05.072.

[42] C. Pan and Y. Zhu, "New Type of BiPO4 Oxy-acid salt photocatalyst with high photocatalytic activity on degradation of dye," *Environ. Sci. Technol.*, vol. 44, no. 14, pp. 5570–5574, 2010, doi: 10.1021/es101223n.

[43] X. Li, X. Li, J. Wang, H. Zhai, and X. Chen, "Synthesis of ZnSe microdisks and nanobelts and their visible-light photocatalytic properties," *J. Mater. Sci.*, vol. 52, no. 7, pp. 3821–3830, 2017, doi: 10.1007/s10853-016-0638-5.

[44] J.-S. Hu *et al.*, "Mass Production and High Photocatalytic Activity of ZnS Nanoporous Nanoparticles," *Angew. Chemie*, vol. 117, no. 8, pp. 1295–1299, 2005, doi: 10.1002/ange.200462057.

[45] D. Chen *et al.*, "ZnS nano-architectures: Photocatalysis, deactivation and regeneration," *Nanoscale*, vol. 2, no. 10, pp. 2062–2064, 2010, doi: 10.1039/c0nr00171f.

[46] D. Hu, Y. J. Liu, H. S. Li, X. Y. Cai, X. L. Yan, and Y. D. Wang, "Effect of nickel doping on structural, morphological and optical properties of sol-gel spin coated ZnO films," *Mater. Technol.*, vol. 27, no. 3, pp. 243–250, 2012, doi: 10.1179/1753555712Y.0000000006.

[47] Q. Xiang, J. Yu, and M. Jaroniec, "Enhanced photocatalytic H2-production activity of graphene-modified titania nanosheets," *Nanoscale*, vol. 3, no. 9, pp. 3670–3678, 2011, doi: 10.1039/c1nr10610d.

[48] S. Cho, J. W. Jang, J. S. Lee, and K. H. Lee, "Porous ZnO-ZnSe nanocomposites for visible light photocatalysis," *Nanoscale*, vol. 4, no. 6, pp. 2066–2071, 2012, doi:

10.1039/c2nr11869f.

[49] M. Basu, N. Garg, and A. K. Ganguli, "A type-II semiconductor (ZnO/CuS heterostructure) for visible light photocatalysis," *J. Mater. Chem. A*, vol. 2, no. 20, pp. 7517–7525, 2014, doi: 10.1039/c3ta15446g.

[50] Z. Shi, J. Liu, D. Liu, Q. Zhang, J. Lang, and X. Li, "Preparation and Comparison of the Photocatalytic Properties of ZnSe with Different Crystalline Phases," *Phys. Status Solidi Basic Res.*, vol. 256, no. 8, pp. 1–7, 2019, doi: 10.1002/pssb.201800754.

[51] E. Karamian and S. Sharifnia, "On the general mechanism of photocatalytic reduction of CO2," *J. CO2 Util.*, vol. 16, pp. 194–203, 2016, doi: 10.1016/j.jcou.2016.07.004.

[52] K. Yadav, M. Giri, and N. Jaggi, "Synthesis, characterization and photocatalytic studies of ZnSe and Ag:ZnSe nanoparticles," *Res. Chem. Intermed.*, vol. 41, no. 12, pp. 9967–9978, 2015, doi: 10.1007/s11164-015-2002-9.

[53] J. Zhang, B. Tian, L. Wang, M. Xing, and J. Lei, "Mechanism of Photocatalysis," pp. 1–15, 2018, doi: 10.1007/978-981-13-2113-9_1.

[54] Y. Wang, J. Niu, Z. Zhang, and X. Long, "Sono-photocatalytic degradation of organic pollutants in water," *Prog. Chem.*, vol. 20, no. 10, pp. 1621–1627, 2008.

[55] M. Saranya *et al.*, "Hydrothermal growth of CuS nanostructures and its photocatalytic properties," *Powder Technol.*, vol. 252, pp. 25–32, 2014, doi: 10.1016/j.powtec.2013.10.031.

[56] X. Chen, Y. Dai, and X. Wang, "Methods and mechanism for improvement of photocatalytic activity and stability of Ag3PO4: A review," *J. Alloys Compd.*, vol. 649, pp. 910–932, 2015, doi: 10.1016/j.jallcom.2015.07.174.

[57] H. de Lasa, B. Serrano, M. Salaices, H. de Lasa, B. Serrano, and M. Salaices, "Photocatalysts, Radiation Sources and Auxiliary Equipment for Photocatalysis," *Photocatalytic React. Eng.*, pp. 49–62, 2005, doi: 10.1007/0-387-27591-6_3.

[58] W. Chen, N. Zhang, M. Y. Zhang, X. T. Zhang, H. Gao, and J. Wen, "Controllable growth of ZnO-ZnSe heterostructures for visible-light photocatalysis," *CrystEngComm*, vol. 16, no. 6, pp. 1201–1206, 2014, doi: 10.1039/c3ce42068j.

[59] Z. Wu, H. Wang, Y. Xue, B. Li, and B. Geng, "ZnO nanorods/ZnSe heteronanostructure arrays with a tunable microstructure of ZnSe shell for visible light photocatalysis," *J. Mater. Chem. A*, vol. 2, no. 41, pp. 17502–17510, 2014, doi: 10.1039/c4ta02989e.

[60] F. Qiao, Q. Liang, X. Hou, J. Yang, and Q. Xu, "Two-Step Preparation of ZnO/ZnSe Heterostructure with Remarkable Photocatalytic Activity by Ultrasonic and Hydrothermal Approach," *J. Electron. Mater.*, vol. 48, no. 7, pp. 4418–4423, 2019, doi: 10.1007/s11664-019-07209-3.

[61] L. Mohan, N. Sisupalan, K. Ponnusamy, and S. Sadagopalan, "One Step Synthesis and

Characterization of ZnO–ZnSe Heterostructures by Chemical Precipitation and Its Solar Photocatalytic Activity," *J. Inorg. Organomet. Polym. Mater.*, vol. 30, no. 7, pp. 2626–2632, 2020, doi: 10.1007/s10904-020-01460-6.

[62] Y. J. Jang *et al.*, "Selective CO production by Au coupled ZnTe/ZnO in the photoelectrochemical CO2 reduction system," *Energy Environ. Sci.*, vol. 8, no. 12, pp. 3597–3604, Dec. 2015, doi: 10.1039/c5ee01445j.

[63] "In situ synthesis of ZnO/ZnTe common cation heterostructure and its visible-light photocatalytic reduction of CO2 into CH4 - ScienceDirect." https://www.sciencedirect.com/science/article/pii/S0926337314007711 (accessed Jun. 13, 2021).

[64] G. Hitkari, S. Singh, and G. Pandey, "Structural, optical and photocatalytic study of ZnO and ZnO–ZnS synthesized by chemical method," *Nano-Structures and Nano-Objects*, vol. 12, pp. 1–9, 2017, doi: 10.1016/j.nanoso.2017.08.007.

[65] U. Diebold, "<(Surf.Sci.Rep.)[2003]The surface science of titanium dioxide.pdf>," *Surf. Sci. Rep.*, vol. 48, no. 1, pp. 53–229, 2002, [Online]. Available: http://linkinghub.elsevier.com/retrieve/pii/S0167572902001000.

[66] V. Subramanian, E. E. Wolf, and P. V. Kamat, "Catalysis with TiO2/Gold Nanocomposites. Effect of Metal Particle Size on the Fermi Level Equilibration," *J. Am. Chem. Soc.*, vol. 126, no. 15, pp. 4943–4950, 2004, doi: 10.1021/ja0315199.

[67] Y. Bessekhouad, D. Robert, and J. V. Weber, "Bi2S3/TiO2 and CdS/TiO2 heterojunctions as an available configuration for photocatalytic degradation of organic pollutant," *J. Photochem. Photobiol. A Chem.*, vol. 163, no. 3, pp. 569–580, 2004, doi: 10.1016/j.jphotochem.2004.02.006.

[68] M. Xie, X. Fu, L. Jing, P. Luan, Y. Feng, and H. Fu, "Long-lived, visible-light-excited charge carriers of TiO 2/BiVO4 nanocomposites and their unexpected photoactivity for water splitting," *Adv. Energy Mater.*, vol. 4, no. 5, pp. 4–9, 2014, doi: 10.1002/aenm.201300995.

[69] S. Cho, J. W. Jang, J. Kim, J. S. Lee, W. Choi, and K. H. Lee, "Three-dimensional type II ZnO/ZnSe heterostructures and their visible light photocatalytic activities," *Langmuir*, vol. 27, no. 16, pp. 10243–10250, 2011, doi: 10.1021/la201755w.

[70] G. Dai, S. Liu, Y. Liang, and T. Luo, "Synthesis and enhanced photoelectrocatalytic activity of p-n junction Co 3 O 4 /TiO 2 nanotube arrays," *Appl. Surf. Sci.*, vol. 264, pp. 157–161, 2013, doi: 10.1016/j.apsusc.2012.09.160.

[71] J. Zhang, S. Z. Qiao, L. Qi, and J. Yu, "Fabrication of NiS modified CdS nanorod p-n junction photocatalysts with enhanced visible-light photocatalytic H2-production activity," *Phys. Chem. Chem. Phys.*, vol. 15, no. 29, pp. 12088–12094, 2013, doi: 10.1039/c3cp50734c.

[72] M. Wang, L. Sun, Z. Lin, J. Cai, K. Xie, and C. Lin, "P-n Heterojunction photoelectrodes composed of Cu2O-loaded TiO2 nanotube arrays with enhanced

photoelectrochemical and photoelectrocatalytic activities," *Energy Environ. Sci.*, vol. 6, no. 4, pp. 1211–1220, 2013, doi: 10.1039/c3ee24162a.

[73] S. Gao, W. Wang, Y. Ni, C. Lu, and Z. Xu, "Facet-dependent photocatalytic mechanisms of anatase TiO2: A new sight on the self-adjusted surface heterojunction," *J. Alloys Compd.*, vol. 647, pp. 981–988, 2015, doi: 10.1016/j.jallcom.2015.06.204.

[74] M. S. Akple *et al.*, "Nitrogen-doped TiO2 microsheets with enhanced visible light photocatalytic activity for CO2 reduction," *Cuihua Xuebao/Chinese J. Catal.*, vol. 36, no. 12, pp. 2127–2134, 2015, doi: 10.1016/S1872-2067(15)60989-5.

[75] W. Wang, D. Xu, B. Cheng, J. Yu, and C. Jiang, "Hybrid carbon@TiO2 hollow spheres with enhanced photocatalytic CO2 reduction activity," *J. Mater. Chem. A*, vol. 5, no. 10, pp. 5020–5029, 2017, doi: 10.1039/c6ta11121a.

[76] D. Xu, B. Cheng, S. Cao, and J. Yu, "Enhanced photocatalytic activity and stability of Z-scheme Ag2CrO4-GO composite photocatalysts for organic pollutant degradation," *Appl. Catal. B Environ.*, vol. 164, pp. 380–388, 2015, doi: 10.1016/j.apcatb.2014.09.051.

[77] F. Paquin, J. Rivnay, A. Salleo, N. Stingelin, and C. Silva, "Multi-phase semicrystalline microstructures drive exciton dissociation in neat plastic semiconductors," *J. Mater. Chem. C*, vol. 3, no. 207890, pp. 10715–10722, 2015, doi: 10.1039/b000000x.

[78] Q. Li *et al.*, "Highly efficient visible-light-driven photocatalytic hydrogen production of CdS-cluster-decorated graphene nanosheets," *J. Am. Chem. Soc.*, vol. 133, no. 28, pp. 10878–10884, 2011, doi: 10.1021/ja2025454.

[79] H. Zhou, Y. Qu, T. Zeid, and X. Duan, "Towards highly efficient photocatalysts using semiconductor nanoarchitectures," *Energy Environ. Sci.*, vol. 5, no. 5, pp. 6732–6743, 2012, doi: 10.1039/c2ee03447f.

[80] S. J. Hong, S. Lee, J. S. Jang, and J. S. Lee, "Heterojunction BiVO4/WO3 electrodes for enhanced photoactivity of water oxidation," *Energy Environ. Sci.*, vol. 4, no. 5, pp. 1781–1787, 2011, doi: 10.1039/c0ee00743a.

[81] I. Tateishi, H. Katsumata, T. Suzuki, and S. Kaneco, "Visible-Light-Induced AgI/Bi7O9I3 Composites with Enhanced Photocatalytic Activity," *Catal. Letters*, vol. 147, no. 6, pp. 1503–1509, 2017, doi: 10.1007/s10562-017-2059-8.

[82] C. Pan, J. Xu, Y. Wang, D. Li, and Y. Zhu, "Dramatic activity of C 3N 4/BiPO 4 photocatalyst with core/shell structure formed by self-assembly," *Adv. Funct. Mater.*, vol. 22, no. 7, pp. 1518–1524, 2012, doi: 10.1002/adfm.201102306.

[83] F. Imtiaz, J. Rashid, and M. Xu, "Semiconductor Nanocomposites for Visible Light Photocatalysis of Water Pollutants," *Concepts Semicond. Photocatal.*, 2019, doi: 10.5772/intechopen.86542.

[84] G. J. Lee and J. J. Wu, "Recent developments in ZnS photocatalysts from synthesis to photocatalytic applications — A review," *Powder Technol.*, vol. 318, pp. 8–22, 2017,

doi: 10.1016/j.powtec.2017.05.022.

[85] F. Vaquero, R. M. Navarro, and J. L. G. Fierro, “Influence of the solvent on the structure, morphology and performance for H2 evolution of CdS photocatalysts prepared by solvothermal method,” *Appl. Catal. B Environ.*, vol. 203, pp. 753–767, 2017, doi: 10.1016/j.apcatb.2016.10.073.

[86] C. Li, J. Yuan, B. Han, and W. Shangguan, “Synthesis and photochemical performance of morphology-controlled CdS photocatalysts for hydrogen evolution under visible light,” *Int. J. Hydrogen Energy*, vol. 36, no. 7, pp. 4271–4279, 2011, doi: 10.1016/j.ijhydene.2011.01.022.

[87] S. Zhang, Q. Chen, Y. Wang, and L. Guo, “Synthesis and photoactivity of CdS photocatalysts modified by polypyrrole,” *Int. J. Hydrogen Energy*, vol. 37, no. 17, pp. 13030–13036, 2012, doi: 10.1016/j.ijhydene.2012.05.060.

[88] J. Xu, W. Wang, X. Zhang, X. Chang, Z. Shi, and G. M. Haarberg, “Electrodeposition of ZnSe thin film and its photocatalytic properties,” *J. Alloys Compd.*, 2015, doi: 10.1016/j.jallcom.2015.01.013.

[89] L. Zhang, H. Yang, X. Xie, F. Zhang, and L. Li, “Preparation and photocatalytic activity of hollow ZnSe microspheres via Ostwald ripening,” *J. Alloys Compd.*, vol. 473, no. 1–2, pp. 65–70, 2009, doi: 10.1016/j.jallcom.2008.06.018.

[90] H. Zhang and Y. Zhu, “Significant visible photoactivity and antiphotocorrosion performance of CdS photocatalysts after monolayer polyaniline hybridization,” *J. Phys. Chem. C*, vol. 114, no. 13, pp. 5822–5826, 2010, doi: 10.1021/jp910930t.

[91] B. Liu, T. Torimoto, and H. Yoneyama, “<PhotoChemPhotoBio_93_1998.pdf>,” no. 97, 1998.

[92] M. V. Kovalenko, M. I. Bodnarchuk, A. L. Stroyuk, and S. Y. Kuchmii, “Spectral, optical, and photocatalytic characteristics of quantum-sized particles of CdTe,” *Theor. Exp. Chem.*, vol. 40, no. 4, pp. 220–225, 2004, doi: 10.1023/B:THEC.0000041806.60632.04.

[93] G. Han *et al.*, “Visible-light photocatalysis in CdTe nanoflakes with exposed {111} facets and charge separation between polar CdTe {111}surfaces,” *Appl. Catal. B Environ.*, vol. 208, no. 111, pp. 94–103, 2017, doi: 10.1016/j.apcatb.2017.02.054.

[94] M. F. Ehsan, M. N. Ashiq, and T. He, “Hollow and mesoporous ZnTe microspheres: Synthesis and visible-light photocatalytic reduction of carbon dioxide into methane,” *RSC Adv.*, vol. 5, no. 8, pp. 6186–6194, 2015, doi: 10.1039/c4ra13593h.

[95] S. Arya, S. Khan, P. Lehana, I. Gupta, and S. Kumar, “Electrical properties of electrodeposited zinc selenide (ZnSe) nanowires,” *J. Mater. Sci. Mater. Electron.*, vol. 25, no. 9, pp. 4150–4155, 2014, doi: 10.1007/s10854-014-2142-5.

[96] R. Yousefi, H. R. Azimi, M. R. Mahmoudian, and W. Jeffrey, “Applied Surface Science The effect of defect emissions on enhancement photocatalytic performance of

ZnSe QDs and ZnSe / rGO nanocomposites," *Appl. Surf. Sci.*, vol. 435, pp. 886–893, 2018, doi: 10.1016/j.apsusc.2017.11.183.

[97] S. Bayat, A. Sobhani, and M. Salavati, "Co 2 SiO 4 nanostructures / nanocomposites : synthesis and investigations of optical , magnetic , photocatalytic , thermal stability and flame retardant properties," *J. Mater. Sci. Mater. Electron.*, vol. 0, no. 0, p. 0, 2018, doi: 10.1007/s10854-018-8695-y.

[98] S. Bayat, D. Ghanbari, and M. Salavati-niasari, "Pechini synthesis of Co 2 SiO 4 magnetic nanoparticles and its application in photo-degradation of azo dyes," *J. Mol. Liq.*, vol. 220, pp. 223–231, 2016, doi: 10.1016/j.molliq.2016.04.066.

[99] Y. Chen and D. D. Dionysiou, "Effect of calcination temperature on the photocatalytic activity and adhesion of TiO2 films prepared by the P-25 powder-modified sol-gel method," *J. Mol. Catal. A Chem.*, vol. 244, no. 1–2, pp. 73–82, 2006, doi: 10.1016/j.molcata.2005.08.056.

[100] Q. Zhang, L. Gao, and J. Guo, "Effects of calcination on the photocatalytic properties of nanosized TiO2 powders prepared by TiCl4 hydrolysis," *Appl. Catal. B Environ.*, vol. 26, no. 3, pp. 207–215, 2000, doi: 10.1016/S0926-3373(00)00122-3.

[101] A. B. Sifontes, M. Rosales, F. J. Méndez, O. Oviedo, and T. Zoltan, "Effect of calcination temperature on structural properties and photocatalytic activity of ceria nanoparticles synthesized employing chitosan as template," *J. Nanomater.*, vol. 2013, 2013, doi: 10.1155/2013/265797.

[102] S. M. Gupta and M. Tripathi, "A review of TiO2 nanoparticles," *Chinese Sci. Bull.*, vol. 56, no. 16, pp. 1639–1657, 2011, doi: 10.1007/s11434-011-4476-1.

[103] T. An *et al.*, "Structural and photocatalytic degradation characteristics of hydrothermally treated mesoporous TiO2," *Appl. Catal. A Gen.*, vol. 350, no. 2, pp. 237–243, 2008, doi: 10.1016/j.apcata.2008.08.022.

[104] B. Ohtani, Y. Ogawa, and S. Nishimoto, "JPysChemB,101,(1997)3746(アモルファス TiO2).pdf," *J. Phys. Chem. B*, vol. 5647, no. 101, pp. 3746–3752, 1997.

[105] Q. Xiao and L. Ouyang, "Photocatalytic activity and hydroxyl radical formation of carbon-doped TiO2 nanocrystalline: Effect of calcination temperature," *Chem. Eng. J.*, vol. 148, no. 2–3, pp. 248–253, 2009, doi: 10.1016/j.cej.2008.08.024.

[106] Q. Chen, H. Liu, Y. Xin, and X. Cheng, "TiO2 nanobelts - Effect of calcination temperature on optical, photoelectrochemical and photocatalytic properties," *Electrochim. Acta*, vol. 111, pp. 284–291, 2013, doi: 10.1016/j.electacta.2013.08.049.

[107] X. F. Lei *et al.*, "Effect of calcination temperature on the structure and visible-light photocatalytic activities of (N, S and C) co-doped TiO 2 nano-materials," *Appl. Surf. Sci.*, vol. 332, pp. 172–180, 2015, doi: 10.1016/j.apsusc.2015.01.110.

[108] N. Riaz, F. K. Chong, B. K. Dutta, Z. B. Man, M. S. Khan, and E. Nurlaela, "Photodegradation of Orange II under visible light using Cu-Ni/TiO 2: Effect of

calcination temperature," *Chem. Eng. J.*, vol. 185–186, pp. 108–119, 2012, doi: 10.1016/j.cej.2012.01.052.

[109] S. mei FU *et al.*, "Effect of calcination temperature on microstructure and photocatalytic activity of BiOX (X=Cl, Br)," *Trans. Nonferrous Met. Soc. China (English Ed.*, vol. 30, no. 3, pp. 765–773, 2020, doi: 10.1016/S1003-6326(20)65252-9.

[110] M. Sun, P. Guo, M. Wang, and F. Ren, "The effect of calcination temperature on the photocatalytic performance of Bi2MoO6 for the degradation of phenol under visible light," *Optik (Stuttg).*, vol. 199, no. August, p. 163319, 2019, doi: 10.1016/j.ijleo.2019.163319.

[111] S. Chakrabarti and B. K. Dutta, "Photocatalytic degradation of model textile dyes in wastewater using ZnO as semiconductor catalyst," *J. Hazard. Mater.*, vol. 112, no. 3, pp. 269–278, 2004, doi: 10.1016/j.jhazmat.2004.05.013.

[112] M. R. Delsouz Khaki, M. S. Shafeeyan, A. A. A. Raman, and W. M. A. W. Daud, "Evaluating the efficiency of nano-sized Cu doped TiO2/ZnO photocatalyst under visible light irradiation," *J. Mol. Liq.*, vol. 258, pp. 354–365, 2018, doi: 10.1016/j.molliq.2017.11.030.

[113] K. M. Reza, A. Kurny, and F. Gulshan, "Parameters affecting the photocatalytic degradation of dyes using TiO2: a review," *Appl. Water Sci.*, vol. 7, no. 4, pp. 1569–1578, 2017, doi: 10.1007/s13201-015-0367-y.

[114] M. Qamar, M. Saquib, and M. Muneer, "Photocatalytic degradation of two selected dye derivatives, chromotrope 2B and amido black 10B, in aqueous suspensions of titanium dioxide," *Dye. Pigment.*, vol. 65, no. 1, pp. 1–9, 2005, doi: 10.1016/j.dyepig.2004.06.006.

[115] N. N. Yunus, F. Hamzah, M. S. So'Aib, and J. Krishnan, "Effect of Catalyst Loading on Photocatalytic Degradation of Phenol by Using N, S Co-doped TiO2," *IOP Conf. Ser. Mater. Sci. Eng.*, vol. 206, no. 1, 2017, doi: 10.1088/1757-899X/206/1/012092.

[116] J. Zhang, B. Tian, L. Wang, and M. Xing, *Photocatalysis*. .

[117] L. C. Macedo, D. A. M. Zaia, G. J. Moore, and H. de Santana, "Degradation of leather dye on TiO2: A study of applied experimental parameters on photoelectrocatalysis," *J. Photochem. Photobiol. A Chem.*, vol. 185, no. 1, pp. 86–93, 2007, doi: 10.1016/j.jphotochem.2006.05.016.

[118] C. C. Wang, C. K. Lee, M. Du Lyu, and L. C. Juang, "Photocatalytic degradation of C.I. Basic Violet 10 using TiO2 catalysts supported by Y zeolite: An investigation of the effects of operational parameters," *Dye. Pigment.*, vol. 76, no. 3, pp. 817–824, 2008, doi: 10.1016/j.dyepig.2007.02.004.

[119] S. Ahmed, "Impact of operating conditions and recent developments in heterogeneous photocatalytic water purification process," *Crit. Rev. Environ. Sci. Technol.*, vol. 42, no. 6, pp. 601–675, 2012, doi: 10.1080/10643389.2010.526492.

[120] X. Li, B. Wei, J. Wang, X. Li, H. Zhai, and D. Wang, "Fabrication and comparison of the photocatalytic activity of ZnSe microflowers and nanosheets," *J. Mater. Sci. Mater. Electron.*, 2015, doi: 10.1007/s10854-015-3519-9.

[121] H. Lin *et al.*, "Synthesis of high-quality brookite TiO 2 single-crystalline nanosheets with specific facets exposed: Tuning catalysts from inert to highly reactive," *J. Am. Chem. Soc.*, vol. 134, no. 20, pp. 8328–8331, 2012, doi: 10.1021/ja3014049.

[122] F. Zuo *et al.*, "Active Facets on Titanium(III)-Doped TiO2: An Effective Strategy to Improve the Visible-Light Photocatalytic Activity," *Angew. Chemie*, vol. 124, no. 25, pp. 6327–6330, 2012, doi: 10.1002/ange.201202191.

[123] J. Li, J. Xu, W. L. Dai, H. Li, and K. Fan, "One-pot synthesis of twist-like helix tungsten-nitrogen-codoped titania photocatalysts with highly improved visible light activity in the abatement of phenol," *Appl. Catal. B Environ.*, vol. 82, no. 3–4, pp. 233–243, 2008, doi: 10.1016/j.apcatb.2008.01.022.

[124] A. K. Benabbou, Z. Derriche, C. Felix, P. Lejeune, and C. Guillard, "Photocatalytic inactivation of Escherischia coli. Effect of concentration of TiO2 and microorganism, nature, and intensity of UV irradiation," *Appl. Catal. B Environ.*, vol. 76, no. 3–4, pp. 257–263, 2007, doi: 10.1016/j.apcatb.2007.05.026.

[125] Y. Li, S. Sun, M. Ma, Y. Ouyang, and W. Yan, "Kinetic study and model of the photocatalytic degradation of rhodamine B (RhB) by a TiO2-coated activated carbon catalyst: Effects of initial RhB content, light intensity and TiO2 content in the catalyst," *Chem. Eng. J.*, vol. 142, no. 2, pp. 147–155, 2008, doi: 10.1016/j.cej.2008.01.009.

[126] A. B. Djurišić, Y. H. Leung, and A. M. Ching Ng, "Strategies for improving the efficiency of semiconductor metal oxide photocatalysis," *Mater. Horizons*, vol. 1, no. 4, pp. 400–410, 2014, doi: 10.1039/c4mh00031e.

[127] A. O. Ibhadon and P. Fitzpatrick, "Heterogeneous photocatalysis: Recent advances and applications," *Catalysts*, vol. 3, no. 1, pp. 189–218, 2013, doi: 10.3390/catal3010189.

[128] P. Singh, P. Shandilya, P. Raizada, A. Sudhaik, A. Rahmani-Sani, and A. Hosseini-Bandegharaei, "Review on various strategies for enhancing photocatalytic activity of graphene based nanocomposites for water purification," *Arab. J. Chem.*, vol. 13, no. 1, pp. 3498–3520, 2020, doi: 10.1016/j.arabjc.2018.12.001.

[129] F. Huang, A. Yan, and H. Zhao, "Influences of Doping on Photocatalytic Properties of TiO2 Photocatalyst," *Semicond. Photocatal. - Mater. Mech. Appl.*, 2016, doi: 10.5772/63234.

[130] J. Ge, Y. Zhang, Y. J. Heo, and S. J. Park, *Advanced design and synthesis of composite photocatalysts for the remediation of wastewater: A review*, vol. 9, no. 2. 2019.

[131] X. Lin, J. Xing, W. Wang, Z. Shan, F. Xu, and F. Huang, "Photocatalytic activities of heterojunction semiconductors Bi 2O3/BaTiO3: A strategy for the design of efficient combined photocatalysts," *J. Phys. Chem. C*, vol. 111, no. 49, pp. 18288–18293, 2007, doi: 10.1021/jp073955d.

[132] D. Sudha and P. Sivakumar, "Review on the photocatalytic activity of various composite catalysts," *Chem. Eng. Process. Process Intensif.*, vol. 97, pp. 112–133, 2015, doi: 10.1016/j.cep.2015.08.006.

[133] H. X. Wang *et al.*, "One-pot solvothermal synthesis of ZnTe/RGO nanocomposites and enhanced visible-light photocatalysis," *Chinese Chem. Lett.*, vol. 27, no. 9, pp. 1572–1576, 2016, doi: 10.1016/j.cclet.2016.03.003.

[134] M. F. Ehsan, M. N. Ashiq, F. Bi, Y. Bi, S. Palanisamy, and T. He, "Preparation and characterization of SrTiO3-ZnTe nanocomposites for the visible-light photoconversion of carbon dioxide to methane," *RSC Adv.*, vol. 4, no. 89, pp. 48411–48418, 2014, doi: 10.1039/c4ra06828a.

[135] M. F. Ehsan and T. He, "In situ synthesis of ZnO/ZnTe common cation heterostructure and its visible-light photocatalytic reduction of CO2 into CH4," *Appl. Catal. B Environ.*, vol. 166–167, pp. 345–352, 2015, doi: 10.1016/j.apcatb.2014.11.058.

[136] M. F. Ehsan, R. Khan, and T. He, "Visible-Light Photoreduction of CO2 to CH4 over ZnTe-Modified TiO2 Coral-Like Nanostructures," *ChemPhysChem*, vol. 18, no. 22, pp. 3203–3210, 2017, doi: 10.1002/cphc.201700404.

[137] Y. Sun *et al.*, "In situ growth, structure characterization, and enhanced photocatalysis of high-quality, single-crystalline ZnTe/ZnO branched nanoheterostructures," *Nanoscale*, vol. 3, no. 10, pp. 4418–4426, 2011, doi: 10.1039/c1nr10922g.

[138] L. Fatolahi and A. Feizbakhsh, "Preparation of zinc tellurides quantum dots and zinc tellurides/multi-walled carbon nanotubes nanocomposites and photocatalytic activity," *Inorg. Nano-Metal Chem.*, vol. 51, no. 8, pp. 1047–1053, 2021, doi: 10.1080/24701556.2020.1814328.

[139] M. K. Lee *et al.*, "Photocatalyses of Nano-Scaled ZnSe/$TiO_2$ and ZnS/$TiO_2$ Heterojunctions," *Key Eng. Mater.*, vol. 368–372, pp. 1474–1476, 2008, doi: 10.4028/www.scientific.net/kem.368-372.1474.

[140] T. T. ThanhThuy, H. Feng, and Q. Cai, "Photocatalytic degradation of pentachlorophenol on ZnSe/TiO2 supported by photo-Fenton system," *Chem. Eng. J.*, vol. 223, pp. 379–387, 2013, doi: 10.1016/j.cej.2013.03.025.

[141] N. R. Khalid, E. Ahmed, Z. Hong, L. Sana, and M. Ahmed, "Enhanced photocatalytic activity of graphene-TiO2 composite under visible light irradiation," *Curr. Appl. Phys.*, vol. 13, no. 4, pp. 659–663, 2013, doi: 10.1016/j.cap.2012.11.003.

[142] P. Chen *et al.*, "Nitrogen-Doped Graphene / ZnSe Nanocomposites : Hydrothermal Synthesis and Their Enhanced Electrochemical and Photocatalytic Activities," no. 1, pp. 712–719, 2012.

[143] B. Liu, L. Tian, and Y. Wang, "One-pot solvothermal synthesis of ZnSe·x N2H 4/GS and ZnSe/N-GS and enhanced visible-light photocatalysis," *ACS Appl. Mater. Interfaces*, vol. 5, no. 17, pp. 8414–8422, 2013, doi: 10.1021/am401701y.

[144] Z.I.Takai, "Ournal of," *Asian J. Chem.*, vol. 30, no. 18, pp. 2424–2430, 2018.

[145] S. Ma, J. Xue, Y. Zhou, and Z. Zhang, "Photochemical synthesis of ZnO/Ag2O heterostructures with enhanced ultraviolet and visible photocatalytic activity," *J. Mater. Chem. A*, vol. 2, no. 20, pp. 7272–7280, 2014, doi: 10.1039/c4ta00464g.

[146] L. Wang, G. Tian, Y. Chen, Y. Xiao, and H. Fu, "In situ formation of a ZnO/ZnSe nanonail array as a photoelectrode for enhanced photoelectrochemical water oxidation performance," *Nanoscale*, vol. 8, no. 17, pp. 9366–9375, 2016, doi: 10.1039/c6nr01969b.

[147] A. R. Khataee, M. Hosseini, Y. Hanifehpour, M. Safarpour, and S. W. Joo, "Yb-Doped ZnSe Nanoparticles : Synthesis , Physical," pp. 6950–6956, 2014, doi: 10.1166/jnn.2014.8937.

[148] A. R. Khataee, M. Hosseini, Y. Hanifehpour, M. Safarpour, and S. W. Joo, "Hydrothermal synthesis and characterization of Nd-doped ZnSe nanoparticles with enhanced visible light photocatalytic activity," *Res. Chem. Intermed.*, vol. 40, no. 2, pp. 495–508, 2014, doi: 10.1007/s11164-012-0977-z.

[149] W. Shi, J. Shi, S. Yu, and P. Liu, "Ion-exchange synthesis and enhanced visible-light photocatalytic activities of CuSe-ZnSe flower-like nanocomposites," *Appl. Catal. B Environ.*, vol. 138–139, pp. 184–190, 2013, doi: 10.1016/j.apcatb.2013.02.031.

[150] Y. Yang *et al.*, "Article Nano Biomed Eng Synthesis , Optical and Photocatalytic Proper- ties of ZnSe Microspheres / Nanosheets," pp. 107–114, doi: 10.5101/nbe.v3i2.p107-114.1.

[151] S. Prasad, V. Kumar, S. Kirubanandam, and A. Barhoum, *Engineered nanomaterials: Nanofabrication and surface functionalization*. Elsevier Inc., 2018.

[152] A. Hernández-Ramírez and I. Medina-Ramírez, *Photocatalytic semiconductors: Synthesis, characterization, and environmental applications*. 2015.

[153] S. Thiagarajan, A. Sanmugam, and D. Vikraman, "Facile Methodology of Sol-Gel Synthesis for Metal Oxide Nanostructures," *Recent Appl. Sol-Gel Synth.*, pp. 1–16, 2017, doi: 10.5772/intechopen.68708.

[154] M. Aliofkhazraei, *Handbook of nanoparticles*. 2015.

[155] A. V. Rane, K. Kanny, V. K. Abitha, and S. Thomas, *Methods for Synthesis of Nanoparticles and Fabrication of Nanocomposites*. Elsevier Ltd., 2018.

[156] Y. X. Gan, A. H. Jayatissa, Z. Yu, X. Chen, and M. Li, "Hydrothermal Synthesis of Nanomaterials," *J. Nanomater.*, vol. 2020, 2020, doi: 10.1155/2020/8917013.

[157] Q. Sun, T. Cheng, Z. Liu, and L. Qi, "A cobalt silicate modified BiVO4 photoanode for efficient solar water oxidation," *Appl. Catal. B Environ.*, vol. 277, no. March, 2020, doi: 10.1016/j.apcatb.2020.119189.

[158] N. A. S. S. Thamizharasan*, "Journal of nanoscience and technology," *J. Nanosci. Technol.*, vol. 5, no. 1, pp. 237–239, 2017, [Online]. Available: http://jacsdirectory.com/journal-of-nanoscience-and-technology/articleview.php?id=67.

[159] K. Senthilkumar, T. Kalaivani, S. Kanagesan, V. Balasubramanian, and J. Balakrishnan, "Wurtzite ZnSe quantum dots: Synthesis, characterization and PL properties," *J. Mater. Sci. Mater. Electron.*, vol. 24, no. 2, pp. 692–696, 2013, doi: 10.1007/s10854-012-0796-4.

[160] A. Salem, E. Saion, N. M. Al-Hada, H. M. Kamari, A. H. Shaari, and S. Radiman, "Simple synthesis of ZnSe nanoparticles by thermal treatment and their characterization," *Results Phys.*, vol. 7, no. March, pp. 1175–1180, 2017, doi: 10.1016/j.rinp.2017.03.011.

[161] W. Xu *et al.*, "Nanoporous CuS with excellent photocatalytic property," *Sci. Rep.*, vol. 5, pp. 1–11, 2015, doi: 10.1038/srep18125.

[162] H. Cui, M. Zayat, and D. Levy, "Effect of HCl on the PPO assisted sol-gel synthesis of olivine-type Co 2 SiO 4 ultrafine particles," pp. 83–87, 2006, doi: 10.1007/s10971-006-8216-y.